Arabian Journal for Science and Engineering
https://doi.org/10.1007/s13369-018-3547-x

AI.1.2

RESEARCH ARTICLE - CIVIL ENGINEERING

Hanging Wall and Footwall Effects in the Largest Reverse-Slip Earthquake of Turkey, October 23, 2011, M_W 7.2 Van Earthquake

Kemal Beyen[1]

Received: 23 March 2018 / Accepted: 2 September 2018
© King Fahd University of Petroleum & Minerals 2018

Abstract
This study provides an engineering-focused assessment of the ground motions recorded during the M_w 7.2 reverse-slip Van earthquake. Spatial and temporal distributions of the site responses and their effects on the structural responses were discussed. Reverse/oblique earthquake characteristics with coupled effects of source, path of propagation and local site conditions in the fault-normal and fault-parallel directions on hanging wall and footwall blocks are particularly considered. Magnitude and distance dependency of the recordings from 22 stations were examined using ground motion prediction equations developed for reverse mechanism. Results show that parameters in the ground motion prediction expressions are not robust enough to represent the source process and propagation effects. Elastic and inelastic displacement limits for the first three closest stations are exceeded in each direction for structural periods greater than about 0.2 s. Severely damaged towns Erciş and Van were examined in the lights of available recordings. Large structural displacement responses of the majority of the buildings initiated inelastic behavior during the main shock. As a consequence of severe demands, structural collapses observed at the region due to poor construction quality which satisfied neither nominal nor full ductility levels. Overall results indicated that effects of directivity and hanging wall effect increased the influence of the seismic loading on structures despite low peak acceleration values recorded at the region. For known active tectonic regions, earthquake design spectrum should be modified over a period range of interest for rupture dynamics and near-fault ground motions in strike-normal and strike-parallel directions.

Keywords Reverse fault · Van earthquake · Directivity effect · Hanging wall · Near-fault effect · Design spectrum

1 Introduction

A M_w 7.2 earthquake occurred on a reverse fault with a relatively shallow focal depth and hit the Van region of the eastern part of Turkey on 23 October 2011 at 10:41 UTC. It is the largest earthquake produced by a thrust fault system in Turkey in the instrumental period until now [1]. Everek erosional thrust fault located in the collision tectonic regime of the Eurasia and Arabian plates in the Anatolian mainland. Processing of a large number of strong motion recordings in both fault-normal (FN) and fault-parallel (FP) directions show systematic differences between hanging wall and footwall sites. Hanging wall effects are observed as the increase in ground motion peaks at short rupture distances for the stations on the hanging wall site and such increments are not seen at the same closest distance stations on the footwall site. The hanging wall effect is caused by a combination of radiation pattern, source directivity and the entrapment of seismic waves within the hanging wall wedge of the fault [2]. Most of the fatalities and damage occurred in the many districts of Erciş on hanging wall block and suburbs of Van did not show striking resemblance between the values of the ground motion parameters and damage distribution.

The most common building construction in the Van region is reinforced concrete (RC) bending moment shear-resisting structure with hollow brick infill walls. Fundamental periods of the buildings vary between 0.2 and 1 s depending upon the number of stories and the construction quality. In this broad range of the structural period, seismic demand imposed by the severe earthquake escalates to high level of intensities and it becomes risk for sensitive buildings with sufficient margin of safety. Surprisingly low peak ground acceleration (PGA) earthquake hit the town of Erciş in the near-field region and the town received a very questionable severe damage possibly due to poor quality construction

✉ Kemal Beyen
kbeyen@kocaeli.edu.tr

[1] Department of Civil Engineering, Kocaeli University, Umuttepe, 41380 Izmit, Kocaeli, Turkey

Published online: 12 September 2018

materials, lack of implementation of design codes, inadequate reinforcement and poor workmanship. Damage, which is more severe and widespread in the central part and less severe as going east and west from the town center, manifests the directivity effect. The main shock recorded at the Muradiye station (6503) had moderate intensity and proper interpretation of such intensity is difficult to explain the damage potential. Another issue to be discussed is that the city of Bitlis-dsi station (1302) in the rupturing directivity zone received extremely higher amplitudes despite its far distance from the epicenter. Because source mechanism and fault rupture are very complex phenomena, there remain a number of questions concerning the characterization of the spatial effects, interpretation and the evaluation of design specifications for reverse fault effects. Coupled effects of source, path of propagation, and site conditions significantly modify the characteristics of an earthquake motion in the propagation field. Strong motion characteristics at the free field demonstrate significant influence of certain source factors such as fault type, fault orientation, rupture mechanism, and directivity of rupturing as well as local site conditions. In order to find answers to all these issues, effects of the earthquake physics on engineering design and common aspects of practice in assessment of the structural performance were studied by Beyen and Tanırcan [2], with emphasis on characteristics of the strong ground motion data of the Van earthquake.

Although the seismic design codes were reflecting the up-to-date experiences and knowledge, many vitally important factors and potential precursory signs have not been considered in the studies of past large destructive earthquakes of the subduction zone in the Anatolian plate. Technically, catastrophic pictures were mainly explained in the literature by substandard construction practice, common structural deficiencies in design, material quality [3] or inadequate performance of the structural system [4–6]. Interpretations of the recordings and geotechnical earthquake engineering aspects were discussed similarly in the literature [7,8]. However, the building codes as a general consensus based on lateral slip fault mechanism earthquake knowledge provide poor indicators or parameters particularly for different earthquake source mechanisms. Therefore, it does not provide comprehensive guidance for revealing some types of damages caused by reverse/oblique fault mechanism. It nevertheless may serve as counterexamples to identify the potential reasons.

In this study, beyond the engineering characteristics of an earthquake, coupled effects of source, path of propagation and local site responses are examined for a thrust tectonic zone in the fault-normal (FN) and fault-parallel (FP) directions on both hanging and footwall blocks. Design spectra and related issues proposed by the Turkish earthquake code (TEC, 2007) are tested for reverse/oblique slip mechanism earthquake by comparison to recorded responses. Study also aims to explain observed intensive structural damage, estimating the earthquake-induced demand and code proposed capacity and help for the implementation of field observations into design practice. Engineering-focused assessments and implications based on extensive number of recordings for the reverse-slip earthquake will help to relate the spatial and temporal distributions of the site responses to the structural responses. Such an assessment will also facilitate to make an accurate decision tree and demonstrate an efficient explanation for the severe damages of the structures, which were designed in fact for the lateral slip fault mechanism earthquakes as declared by the current building codes. The criterion of reliability in engineering design is also considered from the viewpoint of engineering design practice. It is intended to be a bridge between disciplines and practice in an integrated perspective on various engineering parameters to provide a rational basis for designing earthquake-resistant structure.

2 Regional Seismicity

Turkey is located on two minor plates Aegean and Anatolian that is surrounded almost by three major plates, namely, African, Eurasian and Arabian as illustrated in Fig. 1 [9]. In the southeast of Turkey, continental collision converts the northerly movement of the squeezed Anatolian plate with slight rotation toward west about the center of the Anatolian plate producing large strike-slip movements. In the area of Lake Van and further east, active tectonics are dominated by the metamorphic massive of Bitlis (Bitlis suture), Zagros fold and thrust belt. According to GPS studies [10,11], 15 mm/year of 25 mm/year movement of the Arabian plate, is taken up by shortening in the Caucasus, which results in a continental collision along the Bitlis–Zagros fold and thrust belt, this motion is thought to cause intensive seismic activity. The October 23, 2011, Van earthquake occurred in a broad region of convergence beyond the eastern extent of Anatolian strike-slip tectonics. The focal mechanism of the earthquake is characterized by a thrust faulting with a minor left lateral offset [12,13].

It is worth to glance back past regional earthquake activities of the similar tectonic settings in the zone of continental collision. Several activities were recorded in the twentieth century. As major earthquakes of the region, the September 28, 1908, Ms 6.0 Başkale-Van, November 15, 2000, Ms 5.5 Van-Hakkari, and July 2, 2004, Ms 5.1 Doğubayazıt (Karaköse-Ağrı) earthquakes can be remembered for the collision tectonic regime [14,15]. In the 1975 Ms 6.6 Lice-Diyarbakır earthquake, along the length of a 20 km of surface fault rupture, a maximum vertical displacement of about 0.6 m was recorded [16]. The 1976 Ms 7.5 Çaldıran earthquake destroyed 9.232 house-units in Muradiye, Erciş and several districts near Turkey and Iran border, killing about

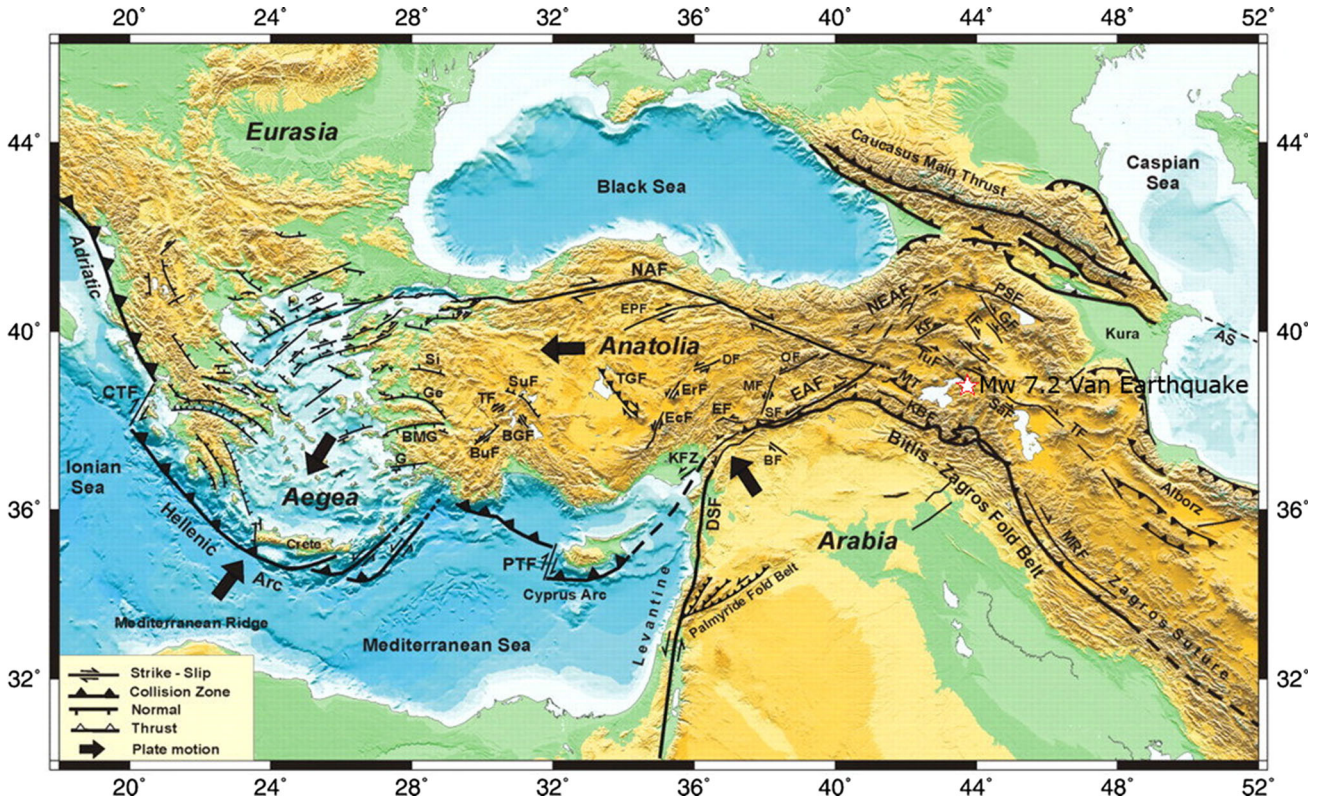


Fig. 1 Large black arrows show relative movement between the Eurasian and Arabian plates and westward movement of the Anatolian and Aegean blocks with respect to Eurasia [9]. NAF: North Anatolian Fault, EAF: East Anatolian Fault, DSF: Dead Sea Fault

Table 1 Damaging earthquakes of the twentieth century in the Van region [19]

Date	Time	Latitude	Longitude	Magnitude
28.04.1903	23:39	39.14	42.65	6.3
06.05.1930	22:34:23	38.22	44.66	7.2
10.09.1941	21:53:57	39.45	43.32	5.9
20.11.1945	06:27:58	38.63	43.33	5.2
25.06.1964	00:11:52	39.13	43.19	5.3
24.11.1976	22:15.6	39.0506	44.0368	7.2
17.01.1977	19:24.7	39.2703	43.7006	5.1
25.06.1988	15:38.3	38.5034	43.0727	5.0
15.11.2000	05:34.9	38.51	43.01	5.7

3.840 people long time after the 1941 Ms 5.9 Erciş earthquake [17]. The 1966 Ms 6.9 Varto earthquake killed 2.394 people. The 1971 Ms 6.8 Bingöl earthquake killed 878 people, devastating 9.111 house-units. The most destructive event 1939 Ms 7.9 Erzincan earthquake struck the city Erzincan killing 32.968 people and destroyed 116.720 house-units [18]. Instrumentally recorded destructive earthquakes ($M \geq 5$) are given in Table 1 with the epicentral locations, date of occurrence and magnitudes [19]. The October 23, 2011, M_w 7.2 Van earthquake is the largest one produced by a reverse fault. A large number of the aftershocks and recent intensive earthquakes triggered nearby faults causing changes in the present regional fault settings, which affect the active stress field, potential strain and release level, potential amounts of seismic slip and rupture area in future activities, therefore directly affect the severity of seismic ground motions. Kandilli Observatory and Earthquake Research Institute, (KOERI), [20] estimated the epicenter of the main shock near Tabanlı village (38.628N, 43.486E). The fault motion suggests that the main shock was generated by a thrust fault within the Bitlis–Zagros fault zone, where thrust mechanism mainly dominates the regional tectonics.

A recent comprehensive study [1] points out that, the source of the 2011 M_w 7.2 Van earthquake is the Everek erosional reverse fault rupturing initiated at the focus inside the earth and propagated out of the earth. Such process resulted in a discontinuous zone of surface rupture with a vertical displacement of 15 cm [1]. In case of the thrust fault, the earthquake epicenter is naturally precessed up from the fault plane and located on the hanging wall block. Seismotectonic map of the Van region and independent earthquakes after the main shock, epicenters, and fault zone are given by Beyen [2]. Ground motion simulation studies show that the N-W dipping plane has strike, dip and rake angles of 241°, 51° and 58°, respectively and when the fault length and width

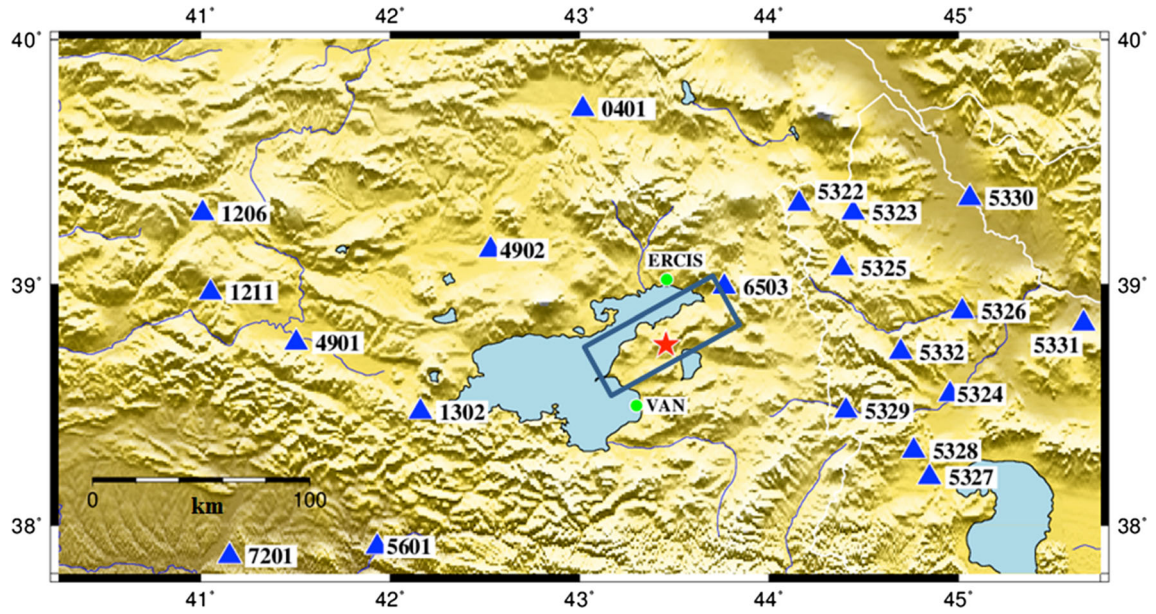


Fig. 2 Location of the regional strong ground motion stations; 6503 Muradiye (r_{epi}: 46.6 km; r_{jb}: 19.5 km), 4902 Malazgirt (r_{epi}: 93.2 km; r_{jb}:74.2 km), 1302 Bitlis-dsi (r_{epi}:111.7 km; r_{jb}:82.8 km), 4901 Muş (r_{epi}:166.5 km; r_{jb}:139.7 km) [19]. Epicenter of the main shock is denoted with a star on the surface projection of the fault plane [21]

are taken as 72 km and 46 km, station-based simulations reasonably estimate the local responses at most of the recording stations [21].

3 Strong Ground Motion Study of the Main Shock

Twenty-two strong ground motion stations of the Earthquake Department of the Disaster and Emergency Management, (AFAD), [19] are considered in this study. Epicentral distances of the regional stations range from 46 to 590 km, with most of them beyond 100 km. Each station holds three-component force-balance accelerometers located at the base of the 2–3 story state houses. Figure 2 depicts available strong motion stations in blue triangles with the station numbers [19]. Epicenter of the main shock is also denoted with a star on the surface projection of the approximate fault rupture plane [21]. Since the rupture direction of the main shock is almost in the E–W direction, it is thought that there is no need to rotate the records for the FN and FP components and the E–W direction is taken as the FP direction. Accordingly, the N–S direction is accepted as the FN for the majority of the records [22]. Because the near-fault region is subjected to large velocity pulses and the site may additionally have a relative static residual displacement (fling effect) due to differential movement between hanging and footwall blocks of a thrust fault system. Data streams are processed in part particularly for the epicentral stations with the intention that it should not destroy or conceal such information. Integration of the accelerogram certainly affects the accuracy of the resultant velocity and displacement time histories at the epicentral stations. Signal processing tool, which is a suite of applications developed in MATLAB [23], performs essential processing such as baseline correction, resampling, and filtering using bidirectional acausal high-pass Butterworth filters at 0.01 Hz. Furthermore, additional band-pass filtering between 0.001 Hz and 50 Hz was also performed to assess the possibility of the fling step, but the findings do not give any substantial support to the static offset.

Strong motion recordings of the epicentral stations Van and Erciş are not available due to technical problems. As an alternative, the Muradiye station (6503) is considered as the nearest strong motion station to the epicenter of the main shock. Muradiye with the distance to the epicenter is approximately same as that of Erciş and received directivity effect more or less same as Erciş. Therefore, the Muradiye station record is examined to explain the highest seismic demand in Erciş as proposed by Konagai [22].

3.1 Magnitude-Distance Characteristics

Magnitude and distance dependency of the strong motion recordings from 22 stations are examined using ground motion prediction equations (GMPE) developed for reverse mechanism systems. Since there is no GMPE consistent with the regional tectonics, it is decided that the statistical prediction may provide practical information on ground motion spatial variability for the towns in the region with no instrumentation. The mechanism of faulting has been included

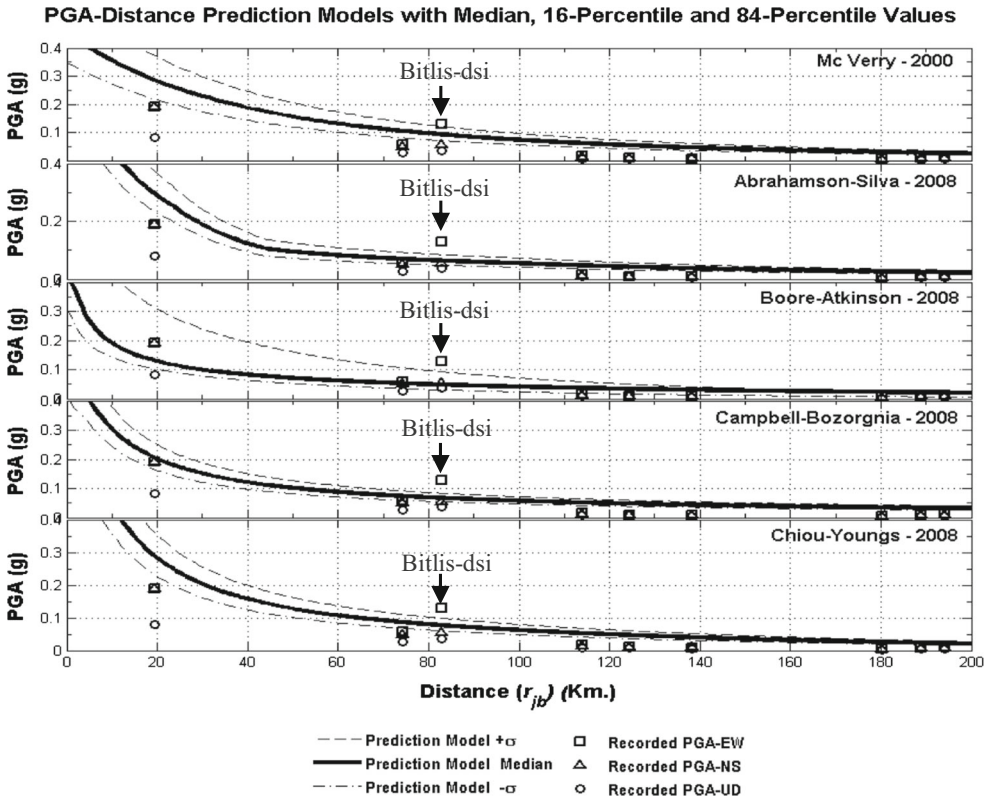


Fig. 3 Estimations of the horizontal PGA-distance dependency curves of the stations within the Joyner–Boore distance of 200 km

as a parameter in the development of some GMPE since it is known that reverse and reverse-oblique mechanisms produce larger motions compared to normal and strike-slip mechanism tectonic regimes [24,25]. From several available types of relationships, recently developed predictive models of Abrahamson and Silva [26], Boore and Atkinson [27], Campbell and Bozorgnia [28], Chiou and Youngs [29] and McVerry [30] are adopted from open-source-Seismic Hazard Analysis [31] and compared with the recordings in Fig. 3. Among commonly used distance measures, the closest horizontal distance to the vertical projection of the rupture (i.e., the Joyner–Boore distance (r_{jb})) is preferred for source to site distances. Figure 3 shows that maxima of ground motions recorded on the two blocks of the thrust fault are different. PGA values of the hanging wall stations are significantly greater than those of footwall stations. The ground motion of the hanging wall station Muradiye with relatively high peaks and many stations with low acceleration peaks such as 3–4 gal within 100 km to 200 km on the footwall block show reverse fault characteristic. An unexpected comparatively large PGA value 10 gal in NS (FN) for the far-field station Muş located next to river bed in the Muş alluvial basin might be evidence of strong influence of the local site characteristics.

From GMPEs of McVerry, Abrahamson–Silva, Boore–Atkinson, Campbell–Bozorgnia and Chiou–Youngs, mean values of PGA are estimated respectively as 0.25 g, 0.3 g, 0.15 g, 0.2 g, 0.28 g for the town of Erciş and the city of Van. Models predicted higher PGA than the recorded values for all the distances. However, Campbell–Bozorgnia model estimates closer as seen in Fig. 3. Most far-field stations (Fig. 2) located on the footwall block recorded small PGA values which are below the mean minus standard deviation ($\mu - \sigma$). Same footwall characteristics can also be pronounced for the epicentral station Van. Thus, PGA value expected for this station should be slightly smaller than the predictions of the models. Horizontal PGA predictions with median, 16-percentile and 84-percentile values may provide the most possible maxima for the malfunctioning station Van, Erciş and other towns in the region. Erciş and Van might be received PGA comparable to Muradiye because of the similarities in source-to-site distance, soil class, propagation effect, and fault zone characteristics [22]. Although Van is located in the fault-normal direction and consequently under the effect of directivity, the PGA value of Van would be lower than the recorded value of Muradiye due to footwall characteristics (see Fig. 2). 'Among the far-field stations as seen in Table 2, largest horizontal PGA value (126.32 gal) was recorded in the EW (FP) component at station Bitlis-dsi located on a stiff soil site.' It manifests ample evidence that the ground motion contains focusing large pulses emanating from the fault as the rupture progresses toward the site. When compared to GMPEs, recorded PGA value is also larger than one standard

Table 2 Peak ground acceleration values for the Van earthquake

Stations		Peak ground acc. (gal)			Epicentral dist. R_{epi} (km)	Joyner–Boore dist. R_{JB} (km)
Code	Name	NS	EW	UD		
6503	Muradiye	− 186.42	186.89	− 79.26	46.6	19.5
4902	Muş	10.06	7.22	4.64	93.2	74.25
1302	Bitlis-dsi	− 54.31	126.32	35.51	116	82.8
401	Ağrı	13.044	15.56	7.219	121	114.0
5601	Siirt	− 9.43	9.38	7.047	158	124.48
4901	Muş	10.05	7.22	4.64	170	138.2
1211	Bingöl_solhan	4.57	− 4.23	2.46	211	180.38
1206	Bingöl_karlıova	7.912	11.11	− 4.66	222	194.07
7201	Batman	− 8.16	7.88	−3.74	223	188.86
2307	Mardin	− 1.98	1.88	−1.58	284	274.13
2305	Elazığ_beyhanioo	1.118	1.33	0.99	289	256.92
2307	Elazığ_palu	2.118	− 1.638	−1.715	307	274.13
2304	Elazığ_kovancılar	1.47	1.69	1.20	313	280.02
2407	Erzincan_tercan	2.45	3.401	2.262	289	264.72
2401	Erzincan	1.533	0.952	− 0.711	358	331.84
6901	Bayburt	1.344	− 1.143	1.275	327	306.17
2902	Gümüşhane_kelkit	− 1.078	−0.879	1.253	378	354.76
6303	Urfa_siverek	2.18	3.054	− 1.602	378	342.91
4404	Malatya_pötürge	1.045	0.946	0.948	405	370.42
205	Adıyaman_kahta	− 3.29	−2.27	− 1.64	437	401.87
208	Adıyaman_gölbaşı	1.074	− 0.767	−0.361	521	484.15
4609	KMaraş	1.761	2.282	0.963	590	552.79

deviation above the mean in EW direction. Only two prediction models Chiou–Youngs [29] and Abrahamson–Silva [26] include one unique parameter for hanging wall as a propagation effect. They estimate noticeably close ground motions within the median $\pm\sigma$ for NS (FN) direction like the others but for the EW (FP) direction, estimations are lower than the recorded PGA value for Bitlis-dsi. Results show that source and propagation parameters of the models do not fully represent the regional characteristics. Therefore, regional empirical spectral amplification model incorporating explicitly the source process and the propagation effects such as rupture directivity, effects of the blocks is necessary for the seismic design as proposed by Shabestari [32] for shallow large magnitude events with a dip-slip faulting like Chi–Chi earthquake.

3.2 Characteristics of the Site Specific Design Spectra

In order to better understand the local response characteristics, building design spectrum are plotted in Figures from 4 to 8 in the form of acceleration, velocity and displacement for 5% damping for representative soil characteristics of the recording sites (i.e., from TEC-2007 [33]; for seismic zone:1, Effective Ground Acceleration Coefficient A_0 :0.4 g, and Local Site Class $Z1$ code proposed design spectrum corner periods T_A and T_B are 0.1 s and 0.3 s respectively.). Spectra in the Figs. 5 through 7 are mainly grouped in two individual characteristics when compared to the compositions. One collection of data profiles, which have too low amplitudes, belong to footwall recording stations and their site responses are considered negligible for design purposes. Therefore, these recording sites are out of the discussion in this study but they can be thought of as a class of footwall data with small amplitudes reflecting general trend. Another collection having larger spectral values shows hanging wall site characteristics. Near field sites on the hanging wall block will be discussed in detail from viewpoint of wave propagation and site responses. In addition to single spectrum plots, tripartite spectra are constructed by combining displacement, velocity and acceleration pseudoresponses into a single graph. The tripartite graph provides a convenient mean to show and examine the relationships in a single chart as seen in Fig. 4. In developing local response spectra, currently employed soil classes of the TEC-2007 [33] are adopted for the sites. Based on the TEC-2007 [33], design spectrum corner periods T_A and T_B vary between 0.1–0.2 and 0.3–0.9 s respectively for different site soil classes. Buildings

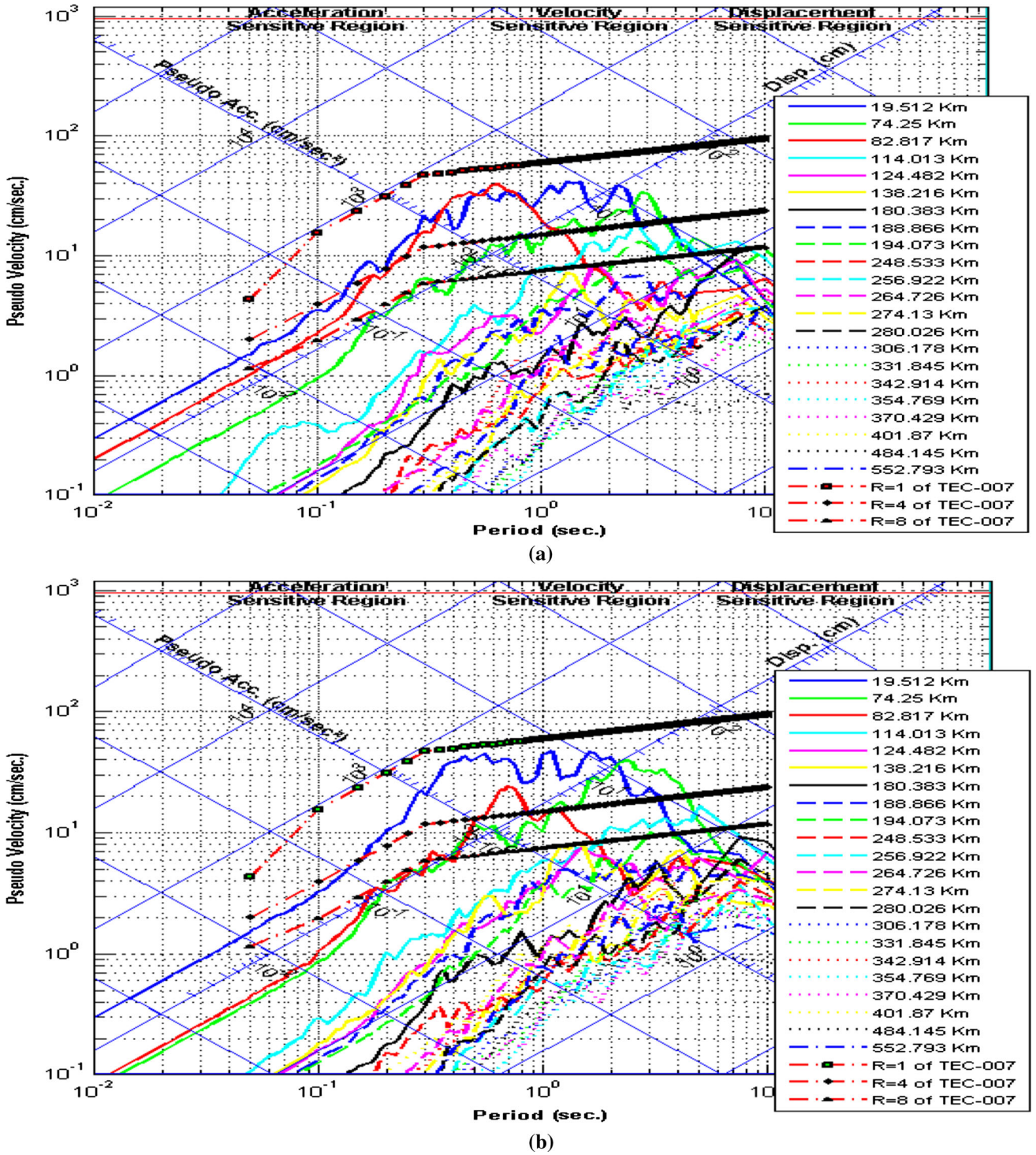
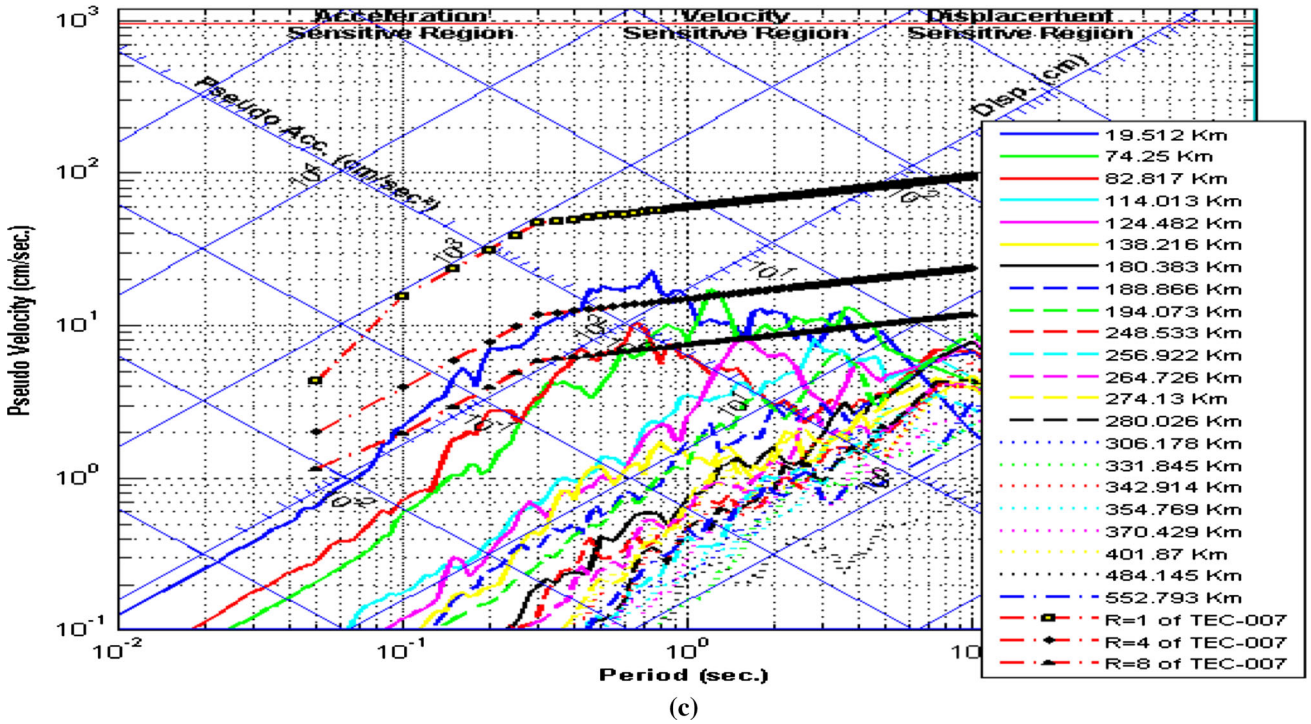


Fig. 4 Tripartite response spectra of the 22 sites (in distances of r_{jb}) and design spectra with different R-values (TEC-2007) [33] for EW, NS and UD from top-down, respectively



(c)

Fig. 4 continued

are designed to have a fraction of the strength required to resist against elastic design forces. This implies that they are expected to undergo inelastic deformation during the design earthquake. Inelastic deformation depends on the ratio of the strength of the structure to the strength required to keep the response within the elastic range and the level of damage should be kept within the structural capacity without collapse. In case, where the required nonlinear behavior should be met for the selected performance level. seismic load reduction factor $R_a(T)$ shall be determined with structural behavior factor R and fundamental period T. R may be equal to 4 for conventional cast-in-situ RC buildings, in which seismic loads are fully resisted by bending moment-shear resisting frames (i.e., with some reserve capacity before reaching yield). R equal to 8 for buildings with high ductility level, experiencing nonlinear post-yielding response without collapse. In this study, for typical ductile buildings representing the majority in the Van region, fundamental periods of the structures are decided to be greater than T_A (0.1–0.2 s), R_a becomes equal to R. The reduced design value $A(T)/R_a(T)$ becomes $A(T)/R$ for elastic non-collapse mechanisms for design based performance level. In the Fig. 4, dashed lines with square, diamond and triangle stand respectively for 1, 4 and 8 for the reduction factor, R_a. It is seen that during the main shock, the spectrum exceeded the reasonable ductility level of many structures and inelastic response might be initiated after consuming reserve capacity at the target ductility. Responses of the majority of the buildings in the region with fundamental periods between 0.3 and 1.0 s need to be considered that they are susceptible to inelastic structural behavior. On the other hand, operational fundamental period should have varied over a large range during the main shock because of the higher mode effects and structural softening in inelastic response.

Acceleration and velocity spectra, when evaluated together, can be utilized to reasonably assess the damage potential of near-fault records. Ground motion characteristics in PSA, PSV and SD at the near-fault station Muradiye and two far fault stations Malazgirt and Bitlis-dsi are also investigated in tripartite plots in Fig. 4. In the FP (EW) component, spectral velocities, (SV), of Muradiye and Bitlis-dsi tracking each other closely are built up progressively for periods up to 1 s while spectral displacements, (SD), are increasing with nearly constant spectral acceleration, (SA). Such trend is also observed for periods up to 3 s for Malazgirt station with lower amplitudes. In the FN (NS) component plotted in Fig. 4b, a similar trend is observed in this case between Bitlis-dsi in the forward/rupturing directivity zone and Malazgirt at the back as a pair of two far end stations. The station Muradiye as the closest one dominates the spectral peaks in both directions. FN component is by far more felt than FP within the same velocity-sensitive region at decreasing SA and with increasing SD. It is understood that spatial variability of the site responses in FP and FN directions shows strong dependence on upcoming wave ronts. Figure 4c shows the spectral quantities for the vertical component. Two far end stations

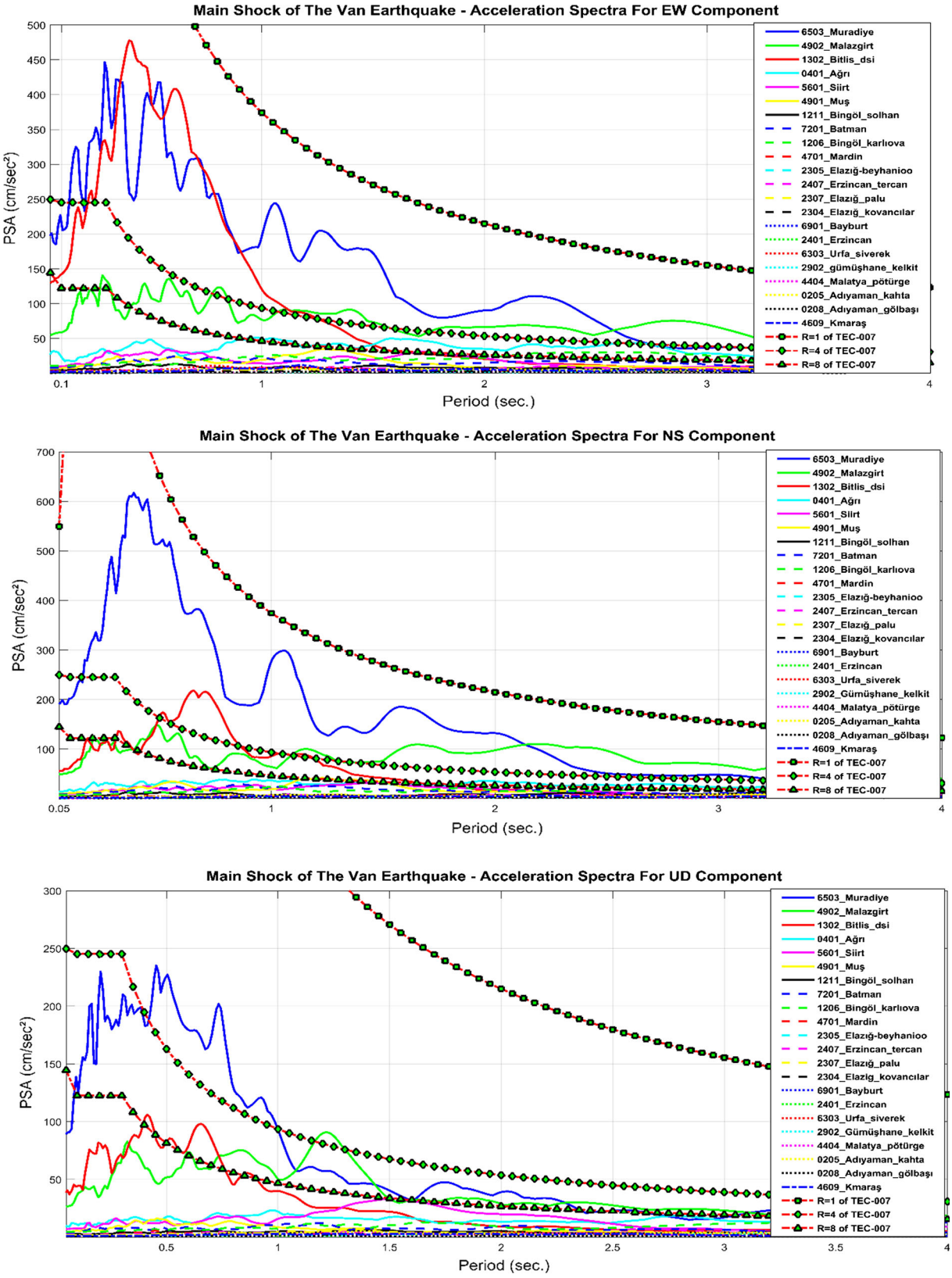


Fig. 5 PSA plots of the main shock data recorded by 22 stations and the design spectra with different R-values ($R = 1, 4, 8$) of the TEC-2007 for horizontal components for EW, NS and UD from top-down, respectively

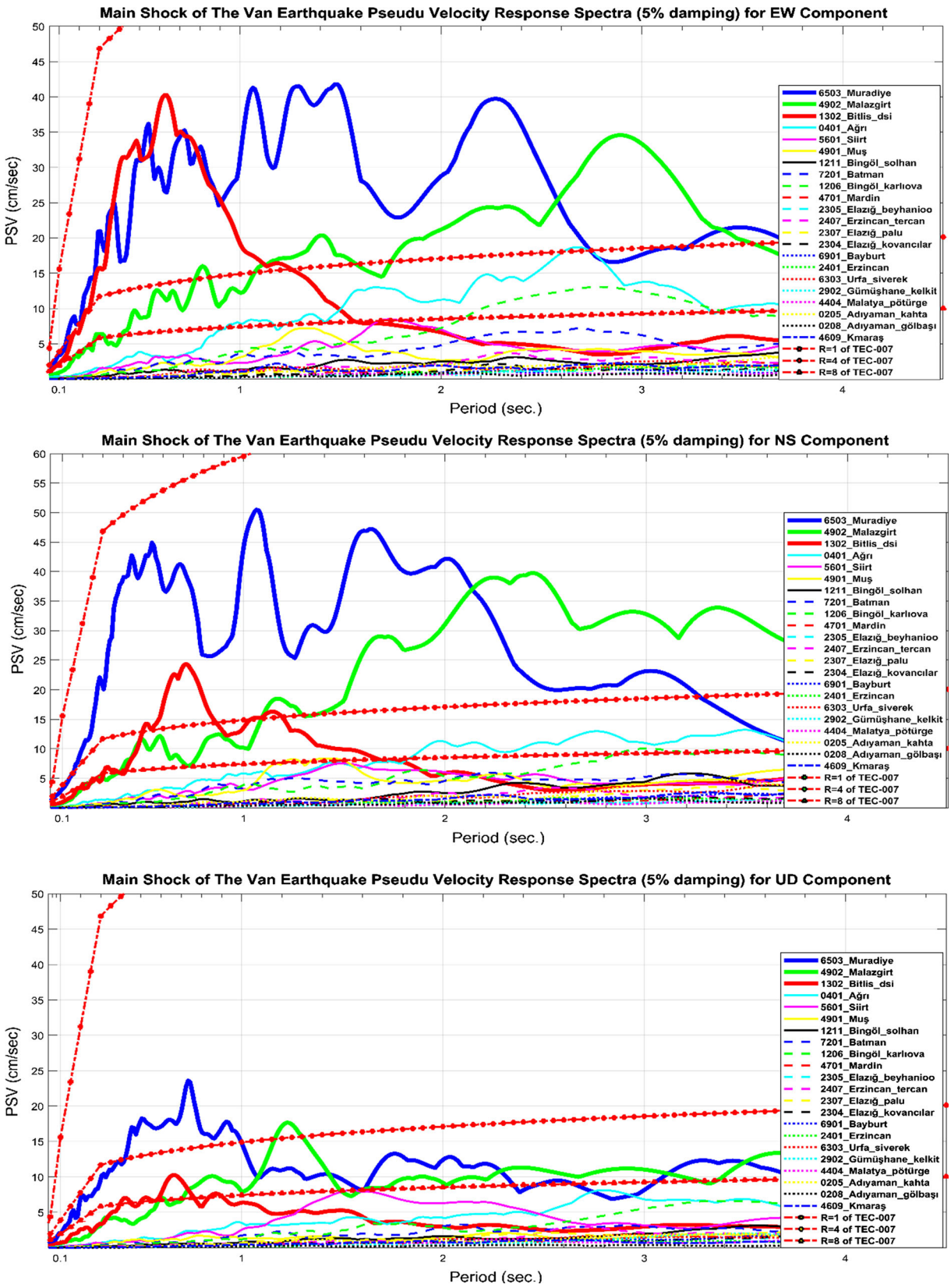


Fig. 6 PSV plots of the main shock data recorded by 22 stations and the velocity design spectra with different R-values ($R = 1, 4, 8$) of the TEC-2007 for horizontal components, EW, NS and UD from top-down, respectively

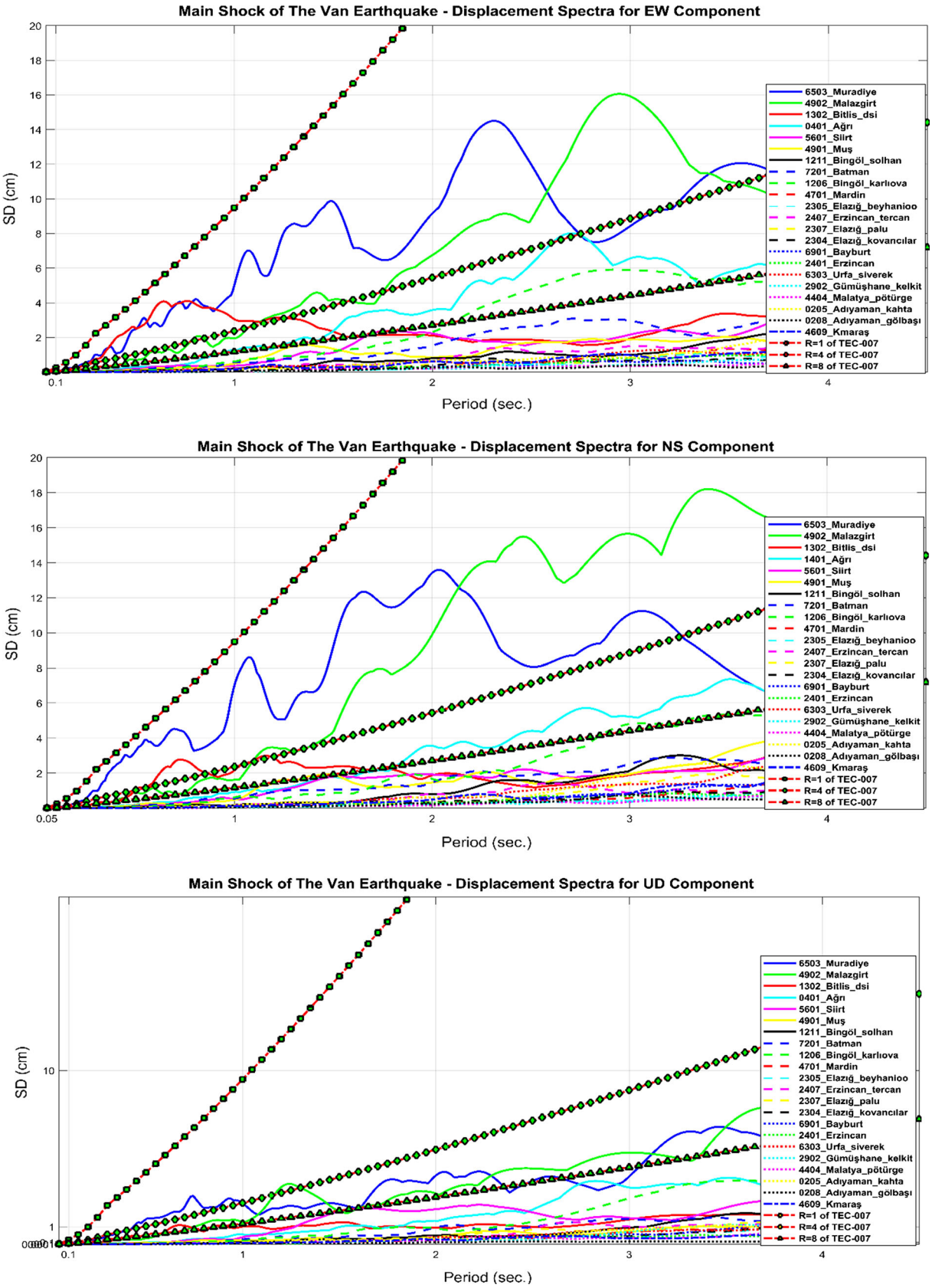


Fig. 7 SD plots of the main shock data recorded by 22 stations and the displacement design spectra with different R-values ($R = 1, 4, 8$) of the TEC-2007 for EW, NS and UD from top-down, respectively

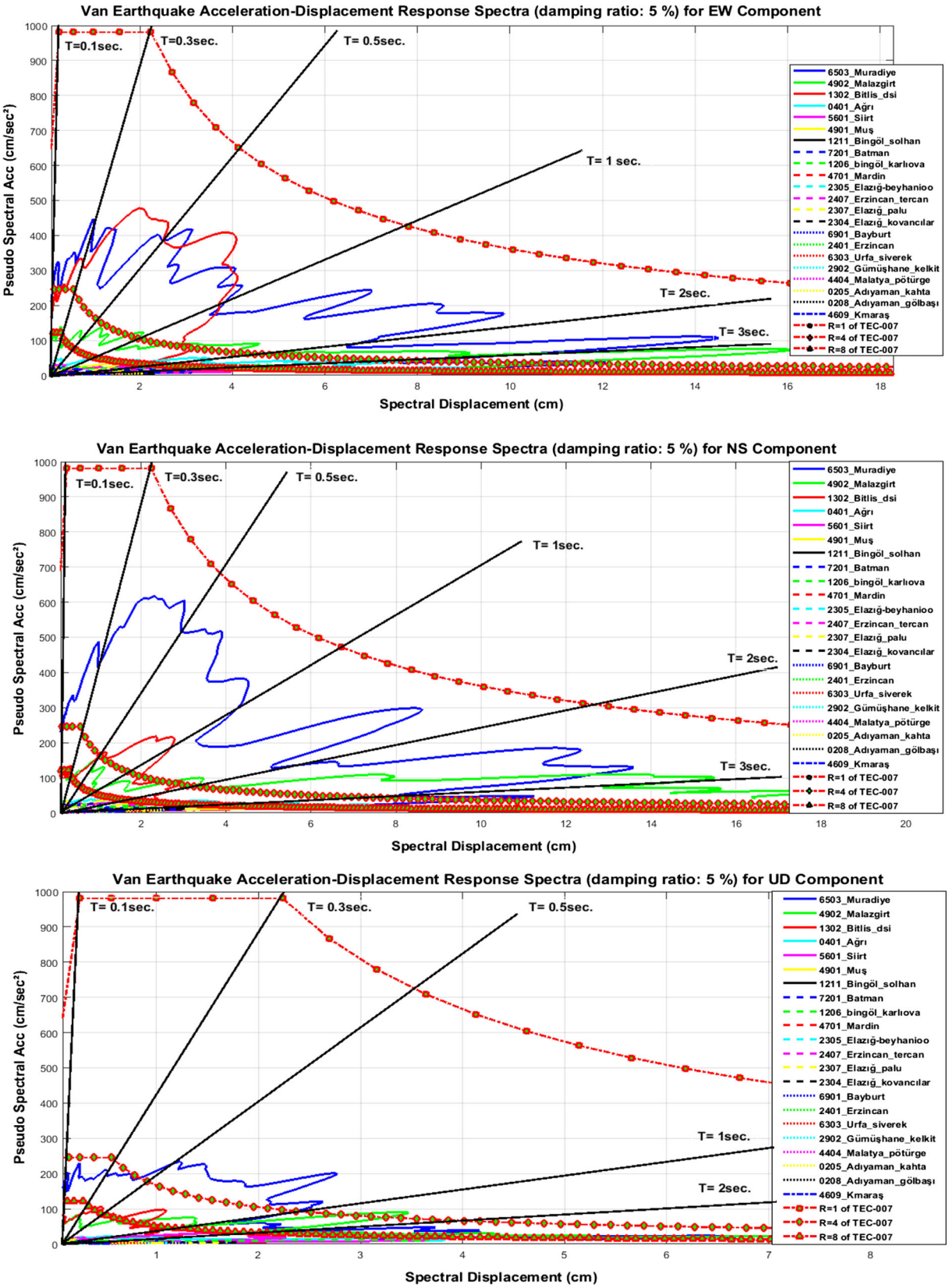


Fig. 8 Demand spectra of the main shock data recorded by 22 stations and PSA-SD design spectra with different R-values ($R = 1, 4, 8$) of the TEC-2007 for EW, NS and UD from top-down, respectively

Muradiye and Bitlis-dsi responded in a similar manner in the first 1 s although Bitlis-dsi is far fault station. Near fault station Muradiye have larger spectral amplitudes up to 1 s. After 1 s, Muradiye and Bitlis-dsi show similar responses up to 7 s.

While the code proposed elastic design spectrum (R-value equals to 1) (TEC, 2007) well envelopes the spectral values computed from records of the main shock, inelastic spectra that are derived by considering the R-values as 4 and 8 are almost exceeded for the periods greater than about 0.2 s. A broad picture of the available values shows that structures in the region were designed for high level of ductility as a usual practice. On the other hand, some may have the construction quality addressing the nominal or high level of ductility. However poor quality construction material, lack of implementation of constructive details such as (i) concrete failure due to lack of confinement, (ii) buckling of the longitudinal reinforcement, (iii) shear failures both within and outside the plastic hinge zone and poor workmanship intensified undesirable failures.

In Figs. 5 and 6, code proposed PSA for typical characteristic structural damping values are identical for structures with very short periods $T < T_A$, whereas the displacements are very small in this acceleration sensitive region as seen in Figs. 4 and 7. Therefore, such structures undergo very little deformations and for the structures with the periods toward T_B, accelerations might be approximately constant at a value equal to amplified ground acceleration depending on damping characteristics of the super- and substructures, consequently depending on impedance ratio at the base mat, input motion may be either increased or decreased. In contrast, structures in the long-period region ($T > T_B$) yield displacement responses approaching to the ground displacements as seen in graphs of Fig. 7. Station Bitlis-dsi and Muradiye received large SD such as 16 cm and 18 cm for EW and NS directions respectively at the peak periods of 2 s and 3 s. It is noteworthy that elastic displacement limits are exceeded in each direction for the first three closest stations (Muradiye and Malazgirt on the hanging wall block and Bitlis-dsi in the rupture directivity). Excessive displacement responses of the majority of the buildings in the epicentral region initiated inelastic behavior during the main shock. This might be an adequate explanation for intensive structural damage of the hanging wall town of Erciş, which has same closest distance to the causative fault comparable to Muradiye. In such a displacement sensitive region, ground acceleration will be very small as appeared in Figs. 4, 5; therefore, structures within the regional periods experienced large story drifts.

In the intermediate period range (design spectrum corner periods approximately between T_A and T_B), which is comparable with the velocity-sensitive region as seen in Figs. 4, 5 and 6, velocity responses of several stations oscillating around moderately constant PSV became unusually narrow and single large peak close to the maximum in FN direction for the city of Bitlis-dsi due to the rupturing effect. Station Muradiye also exhibits PSV in a broad period band up to 3 s for both FN and FP components oscillating around average value of 35 cm/s as seen in Fig. 6. The resultant site-dependent acceleration response spectra do not have a strong influence on the average value of the acceleration in velocity-sensitive region, but it changes the length of the plateau to larger for relatively softer soil conditions in EW (FP) and UD components for the near-fault stations as seen in Fig. 5. In Fig. 7, local displacement responses on hanging and footwall blocks have extreme peak differences in the displacement sensitive region.

Acceleration–displacement response spectrum (ADRS), which was proposed by Fajfar [34] to estimate the design earthquake demand and structural capacity quantities are implemented in this case to discuss the Van earthquake-induced deformation potential for 22 different stations and their environs on both hanging wall and footwall blocks. With 5% damped ADRS as seen in Fig. 8, the influences of nominal ($R = 4$) and high ductility ($R = 8$) level design earthquake forces and recorded seismic forces on moment resisting shear frame buildings are compared based primarily on judgment to account for different hysteretic energy dissipating structures with natural periods of 0.1, 0.3, 0.5, 1, 2, and 3 s. The intersection point between the earthquake demand curve and the capacity proposed by the building code yields pairs, namely earthquake-induced deformation demand (Sd) and peak pseudo acceleration (PSA) demand. These values are tabulated for fault-parallel EW direction in Table 3 as an example.

For 0.1 s period buildings, inelastic design spectrum ($R = 8$) target PSA value 125 cm/s^2 is exceeded 2 times by Muradiye and 1.5 times by Bitlis-dsi. At backward station Malazgirt, earthquake-induced demand is entirely met by the total capacity of the inelastic design. For the buildings with the fundamental period of 0.3 s, PSA inelastic design spectrum ($R = 8$) yielding 125 cm/s^2 is if compared with the earthquake-induced demand values of 450 cm/s^2, 125 cm/s^2 and 325 cm/s^2 for the cities Muradiye, Malazgirt and Bitlis-dsi, respectively. It can be seen for the PSA that earthquake demand was 3 or 4 times the capacity of the inelastic design. Sd values of the three cities namely 1 cm, 0.3 cm and 0.65 cm exceed the inelastic design ($R = 8$) target value of 0.3cm. Same trend is also observed for period equal to 0.5 s and 1 s. In case of 0.5 s period structures, values of Sd 2.5 cm, 0.65 cm and 2.5 cm respectively for Muradiye, Malazgirt and Bitlis-dsi are larger than 0.4 s displacement. For PSA 400/80, 100/80 and 400/80 can be pronounced as a ratio of earthquake demand and inelastic design capacity ratio. Period of 1 s also yields close values as observed from Table 3 and Fig. 8. In case of 2 s and 3 s period buildings, differences

Table 3 Acceleration Displacement Response Spectra for 5% Damping in EW Direction

St. name	T																							
	0.1 s								0.3 s								0.5 s							
	Eq. demand		Design earthquake						Eq. demand		Design earthquake						Eq. demand		Design earthquake					
			Ductility (*R* factor)								Ductility (*R* factor)								Ductility (*R* factor)					
			1		4		8				1		4		8				1		4		8	
	Sd	PSA	Sd	PSA	Sd	PSA	Sd	PSA	Sd	PSA	Sd	PSA	Sd	PSA	Sd	PSA	Sd	PSA	Sd	PSA	Sd	PSA	Sd	PSA
6503_Muradiye	0	250	0.1	981	0	250	0	125	1	450	2,2	981	0.4	250	0.3	125	2.5	400	4.1	640	1	150	0,4	80
4902_Malazgirt	0	125							0.3	125							0.65	100						
1302_Bitlis_dsi	0	180							0.65	325							2.5	400						
St. name	T																							
	1 s								2 s								3 s							
	Eq. demand		Design earthquake						Eq. demand		Design earthquake						Eq. demand		Design earthquake					
			Ductility (*R* factor)								Ductility (*R* factor)								Ductility (*R* factor)					
			1		4		8				1		4		8				1		4		8	
	Sd	PSA	Sd	PSA	Sd	PSA	Sd	PSA	Sd	PSA	Sd	PSA	Sd	PSA	Sd	PSA	Sd	PSA	Sd	PSA	Sd	PSA	Sd	PSA
6503_Muradiye	4	200	7.8	425	2	100	1	50	7	100	7.8	425	2	100	1	50	12	50	25	100	10	50	5	25
4902_Malazgirt	2	110							5	50							14	60						
1302_Bitlis_dsi	4	200							2	25							2	25						

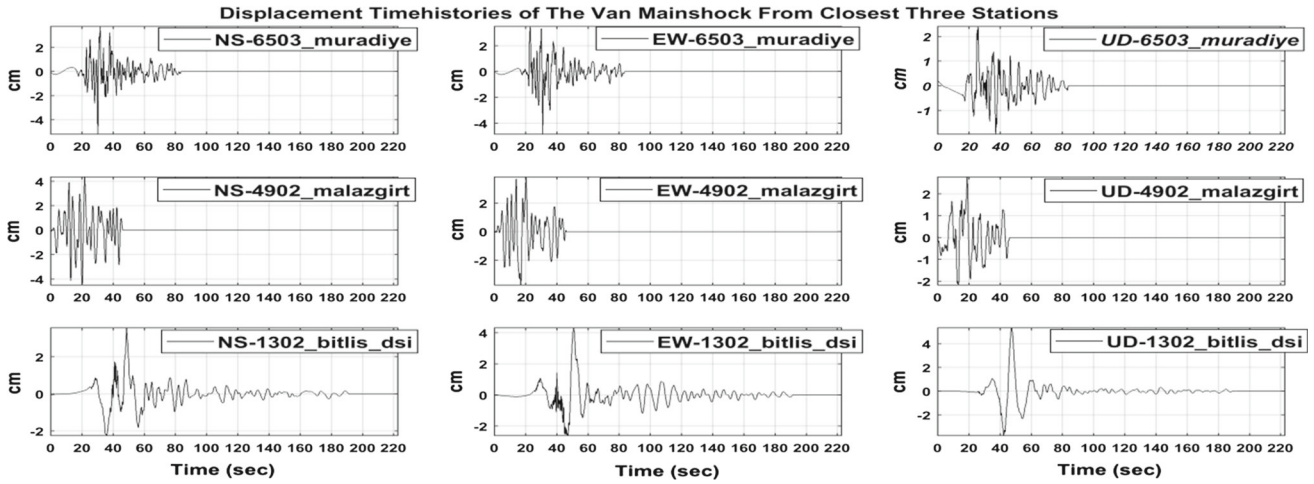


Fig. 9 Displacement time histories of the nearest 3 stations Muradiye, Malazgirt and Bitlis-dsi (from top to bottom), with 3 components NS, EW and UD (from left to right) within 20 s time-grids

between earthquake demand and design targets come to be smaller in PSA but Sd values of inelastic design ($R = 8$) are exceeded many times like 7 and 5 times for the near fault cities Muradiye and Malazgirt. Earthquake-induced Sd and PSA demands marginally larger than design capacity for Bitlis-dsi in fault-parallel direction.

In TEC-2007, the segment before the period equal to 0.3 s is characterized roughly by oscillating values around average constant acceleration and this feature can be seen slightly in the near-field data for EW (fault-parallel) and UD components. Bitlis-dsi (82.817 km) and Muradiye (19.512 km) recordings give very close demand values up to period of 1 s. in EW direction. Such feature is not seen in NS direction. Approximately constantly increasing displacement demands might be pronounced for periods larger than 1 s. In ADRS (Fig. 8) after 1 s, under roughly constant acceleration demand, displacement demands are increasing constantly for the three components. Same trend is also predicted by the design spectra for different ductility levels as the increasing ductility is considered. In PSV spectra, periods between 0.3 and 2–3 s. constant velocity is clearly seen and considered as characteristic for near-fault stations. Code proposed demand spectra used for design is very sensitive to ductility as seen from Figs. 4 and 6. As a general trend, Fig. 8 depicts that displacement component shows typically small values in the short period range and increase up to 18 cm in the long-period region for the Malazgirt station in both horizontal directions whereas station Muradiye exhibits 14 cm structural displacement in long periods for both horizontal directions. Depending on site characteristics, acceleration sensitive region starts very early at small periods for vertical component and later it keeps almost constant up to longer periods. EW (FP) components of the stations Muradiye and Bitlis-dsi near the western edge of the fault show almost similar features for PSA and SD for the periods up to 1 s. In the NS (FN) direction, station Muradiye exhibits the maximum PSA for the periods up to 1 s, further away, in longer period region, peak spectral ground displacements reach up to 14 cm. From acceleration–displacement plot of the Muradiye record, it shows that the structures were undergone excessive accelerations under the effect of the directivity and received severe structural damages, which cause the dominant periods to become longer. In turn, inaccessible large displacements accelerated the collapse mechanism. Local site effects of Erciş and Muradiye towns are if assumed to be approximately same, as described in detail by Ulusay [35] and by Beyen [2], Erciş might be received at least same earthquake and the intensity is built up by the time. Heavy damage and casualties of the town of Erciş with a population of 100,000 citizens can be explained by the effect of forward directivity and site effects, if there is any incomparably higher than that of Muradiye. Moreover, intense velocity and displacement pulses as distinguished from Figs. 9 and 11 characterize near-fault ground motions. These pulses impose severe demands on the structures in near-fault regions. Relatively long-period pulses, which makes near-fault ground motion different from far-field ground motion causes total collapse in near field structures after getting greater the structural period due to large number of member failures.

3.3 Particle Motion Characteristics

In this section, multidimensional features of the ground motions were investigated using particle motion diagrams to show the level of consistency with the findings. In order to protect the multidimensional features, all components are band-pass-filtered at 0.05 Hz and 50 Hz after deciding suitable corner frequency from the Fourier spectra to reduce the

long-period and Nyquist effects. The numbers on the particle motion plots show successive times at every second. The relative amplitudes of the ground motions may be read within the axes limits. The directions of propagations, which are from East to West and from North to South in each component, are stated with initials on the axes. Particle motion plots of the recorded data for the time frame of 10 s. are chosen as extreme examples to show the local site response in three perpendicular planes, which hold the destructive body waves and fatal pulses of the lately arrived surface waves causing partial or total collapse of the structure (damaged for instance from the column-beam connections during the intensive body wave propagation). It is understood that the collapse is triggered by the late surface waves, which are acting as a final cut in failure. Displacement time histories of the nearest 3 stations with 3 components are plotted in Fig. 9 within 20 s time-grids. From EW displacement plots, it is better understood that the rupturing (i.e., source point) started from east end of the fault and propagating toward the west producing rupturing pulses in the wave field while approaching toward the Bitlis-dsi station (i.e., west). This forward directivity effect might be noticed from the first cycle roughly between 40 and 60 s. Same rupturing process is also observed in the station of Malazgirt at the back site. As the source point propagating away from the back station, weakening source effect produces one cycle like displacement between 0 and 40 s, which clearly indicates the backward effect. Short period pulse of Bitlis-dsi and large period pulse of Malazgirt respectively shows the upcoming and weakening rupturing source effect.

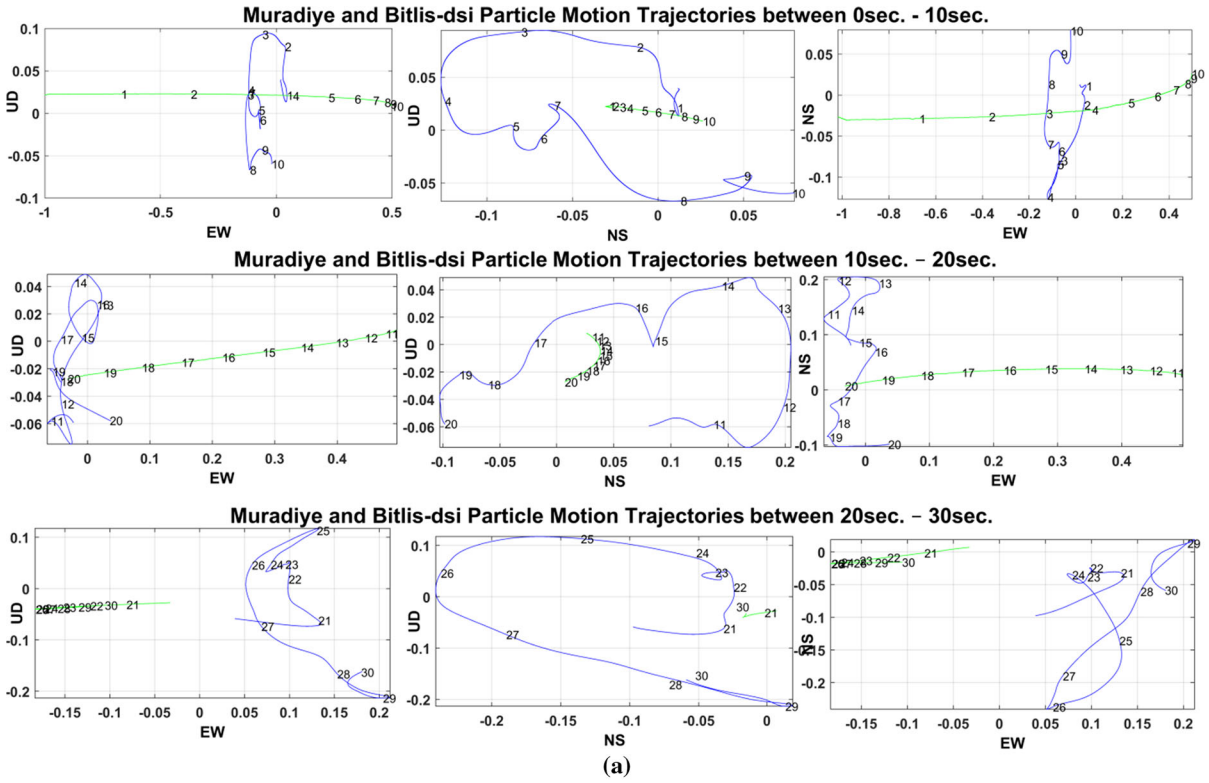
Particle motion plots are given for the towns of Muradiye and Bitlis-dsi in Fig. 10 with the colors of blue and green, respectively. In Fig. 10a, particle motion in the horizontal (NS-EW) plane and two vertical planes UD-NS and UD-EW of the P wave onset is seen in the first 10 s time window of Muradiye record and P wave group in the second 10 s time window in the EW rupturing direction before p wave arriving at the station of Bitlis-dsi. Incidence angle is about 90° for the long-period P-wave oscillation. Between the time window of 20–30 s, SH type body wave is distinguished in the fault-normal direction (NS) in the Muradiye record.

If S-waves are linearly polarized when propagating in homogeneous isotropic medium. Ordinary S-wave particle phase can be observed in the horizontal plane in the 10 s time windows of the Muradiye record through the time segments after 30 s as seen in Fig. 10a. However, in the presence of anisotropy, they split into fast and slow components propagating with different velocity which cause some time delay and related phase shift. Accordingly, the two split S-wave components superimpose to an elliptical polarization as seen in Fig. 10b, if the time windows are extended by adding two time frames one after another, large period polarization in horizontal plane can be recognized between 50 and 70 s. Anisotropy might be confirmed by the elliptical polarization. The orientation of the ellipticity axis and the orientation degree are controlled by the fast and slow velocity directions of the medium with respect to the direction of wave propagation and the level of anisotropy.

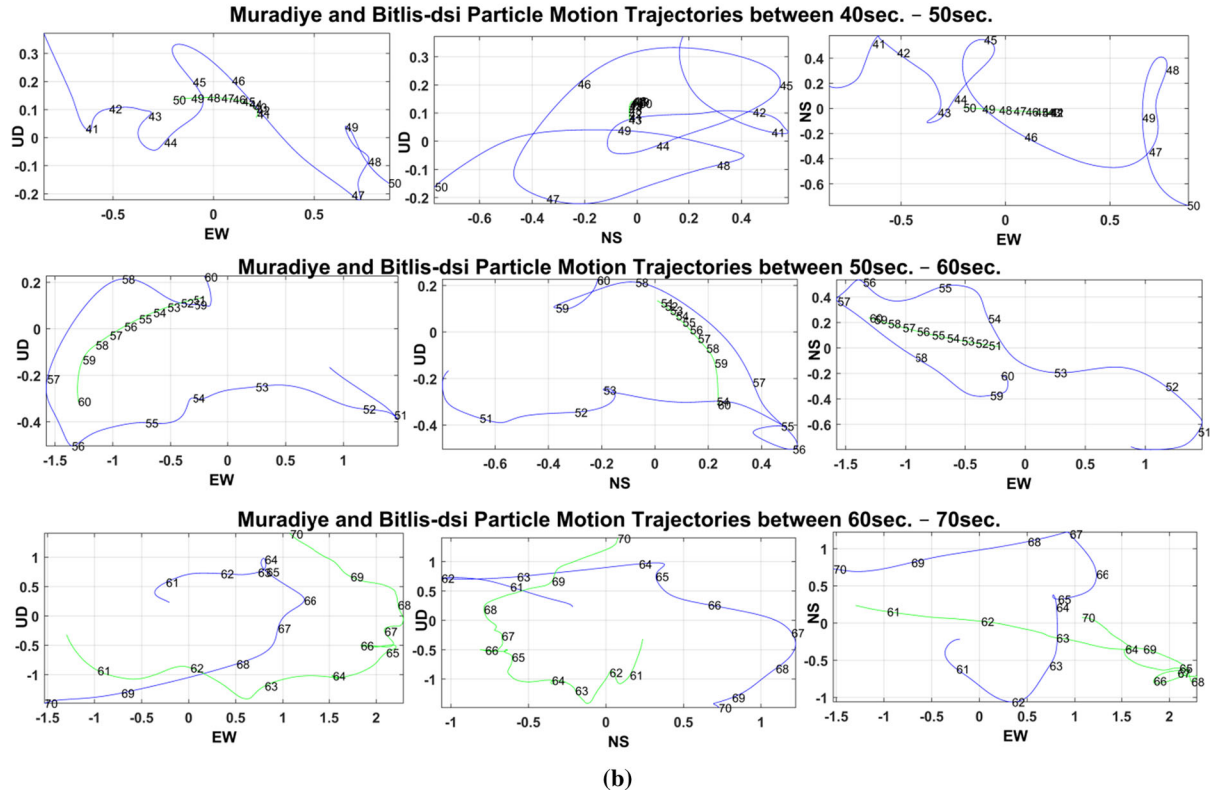
Particle motion interference caused complex particle motion groups. All phases are intermittent therefore certain particle phase might be discussable. SH waves are fully reflected at the free surface. Love waves are formed through constructive interference of repeated reflections of SH at the free surface. For instance, Love like SH might be distinguished roughly from Muradiye record after 60 s. S wave of Bitlis-dsi is appeared in Fig. 10c, while Rayleigh onset in Muradiye is seen in three perpendicular planes in the time frame after 70 s, Love waves and Rayleigh-wave group particle motion trajectories in three perpendicular planes are observed later on. However, it is often difficult to see theoretically expected complete separation of the waves in the real earth structure because of heterogeneity and anisotropy. Coupling of some Rayleigh-wave energy into Love waves and vice versa is possible as seen in Fig. 10d. Long-period effects are observed as good examples of the recording site soil conditions for Bitlis-dsi in Fig. 10d. Three-component displacement time histories at the station Bitlis-dsi in Fig. 9 shows dispersion of surface waves forming long oscillating wave trains up to 200 s.

3.4 Manifestation of Directivity and Rupturing Effect

Main shock data recorded by a few closest stations were used to quantitatively characterize the effect of directivity. In order to see forward rupture directivity in reverse dip-slip events, rupture direction is expected to be aligned up on the fault plane and the slip vectors should point upwards as well. It should not be forgotten that such condition is not often met at normal fault events. The effects occur mostly near the up-dip projection on the surface or the surface rupture. Level of the dip angle changes the fault-normal component. At high dip angles, the strike-normal component can represent the fault-normal component but in cases of low dip angles, the vertical component of recorded ground motion might be pronounced strongly and it may sufficiently represent the fault-normal component [36]. Therefore, horizontal and vertical components might be considered equally in case of any probable error in estimating dip angle. Furthermore, coupled effect is also a reality in practice and should be considered in structural design. A number of studies have shown that relatively stronger velocity pulses in fault-normal ground motion records in the near fault may impose severe demands on structures [37–39]. Such a phenomenon is associated with the rupture from the location of the first energy release toward the site [36,40].



(a)



(b)

Fig. 10 **a** Particle motion trajectories of Muradiye (blue) and Bitlis-dsi (green) for the first three 10 s time windows. **b** Particle motion trajectories of Muradiye (blue) and Bitlis-dsi (green) for 10 s time frames between 40 and 70 s. **c** Particle motion trajectories of Muradiye (blue) and Bitlis-dsi (green) for 10 s time frames between 70 and 90 s. **d** Particle motion trajectories of Muradiye (blue) and Bitlis-dsi (green) for 10 s time frames at three different instants

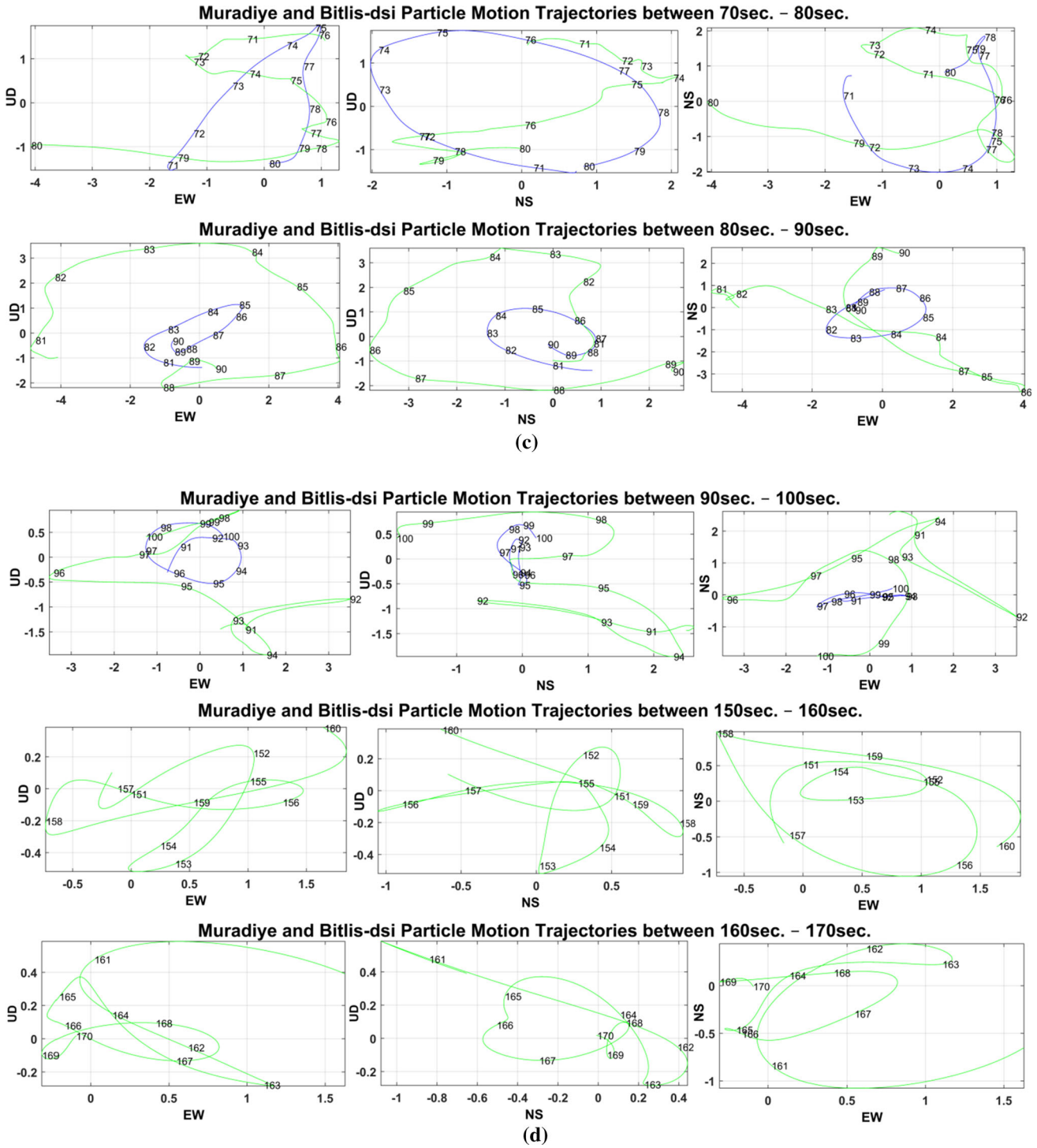


Fig. 10 continued

Figure 11 with insets shows the three component velocity and acceleration time histories recorded at the three closest stations, Muradiye, Bitlis-dsi and Malazgirt on the hanging wall block. Of these, Malazgirt, unfortunately, had only 45 s of recording time with no pre-event set. Reverse and oblique fault mechanisms, depending on dip and rake angles, which are not measurable but approximated indirectly by inversion techniques, may yield complex combination of the rupturing with unique characteristics in both fault-normal and fault-parallel components. It is obvious that the large amplitude in short time duration may indicate intensive damage as observed in the residential regions like the town of Erciş

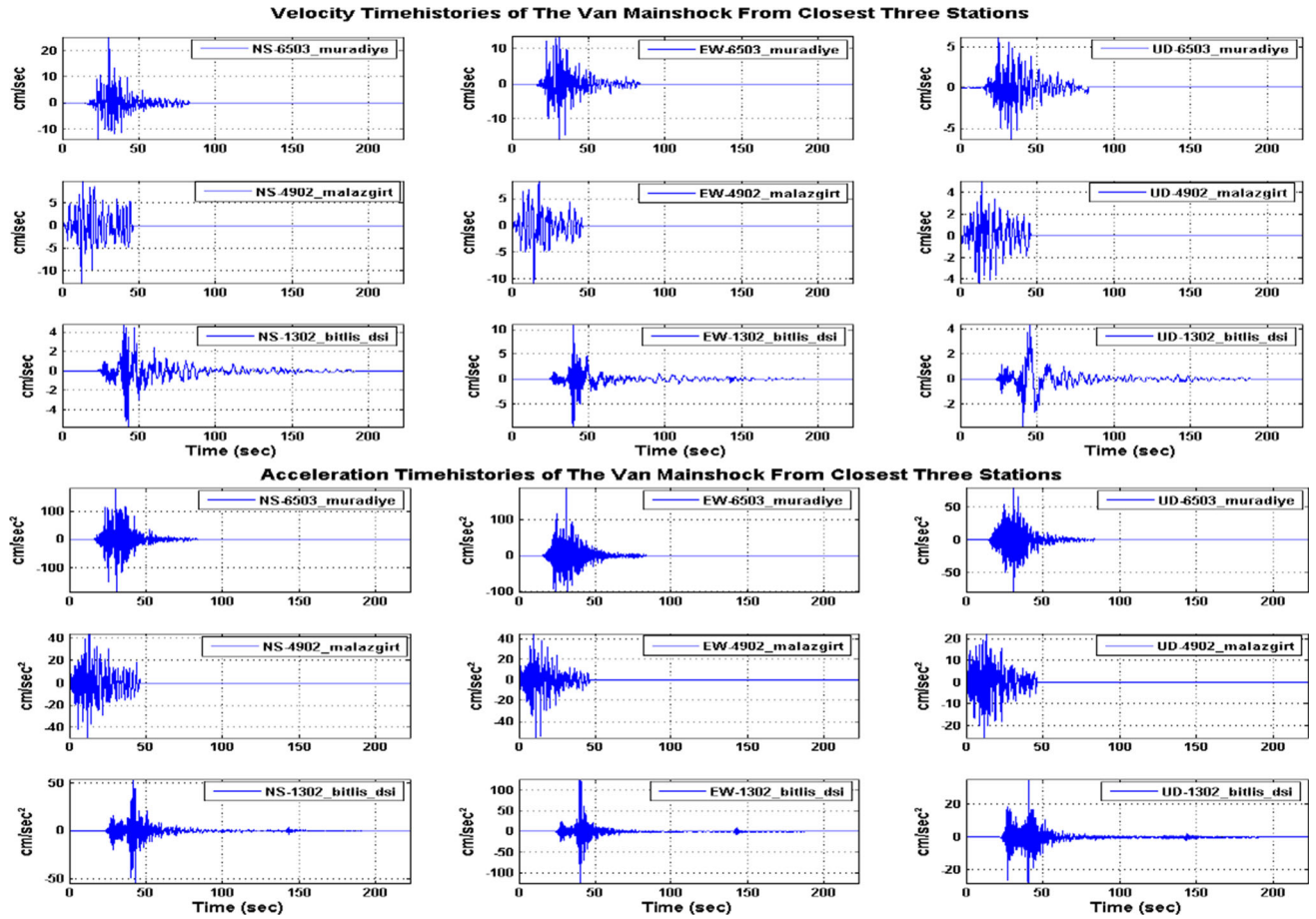


Fig. 11 Three-component velocity (top 3 rows) and acceleration (bottom 3 rows) time histories for the stations Muradiye, Malazgirt and Bitlis-dsi

in the near-source region. If the maximum amplitudes of the recorded accelerations are compared with corresponding components in the r_{jb} distance order; 186 mg (at 19.5 km), 49 mg (at 74 km), 54 mg (at 82.8 km) for NS (FN) direction, 187 mg (at 19.5 km), 56 mg (at 74 km), 102.24 mg (at 82.8 km) for EW (FP) direction, and 79 mg (at 19.5 km), 25 mg (at 74 km), 33 mg (at 82.8 km) for UD direction. Peaks of the station Bitlis-dsi are larger than Malazgirt of the backside and close to the Muradiye in EW (FP) direction. This fact might be explained as a result of total consistency between the direction of slip on the fault plane and the direction of rupture propagating from the center of energy release toward the station Bitlis-dsi. Malazgirt with a single coda shape ground motion with comparatively lower amplitudes reflects the backward directivity effect. Increasing vertical peak ground displacement values such as 2.4 cm, 2.7 cm and 5.3 cm respectively for the stations of Muradiye, Malazgirt, and Bitlis-dsi (see Fig. 9) might be another indication for the earthquake source characteristic. As discussed in Sect. 3.2, short period pulse of Bitlis-dsi (20 s) and large period pulse of Malazgirt (40 s) also show the upcoming and weakening rupturing source effect as observed in Fig. 9. Fault-parallel component velocity time history at Bitlis-dsi shows one dominant ground velocity pulse while perpendicular component recorded many cycles. Peak velocities at Muradiye, Malazgirt and Bitlis-dsi are 25.48 cm/s, 12.7 cm/s and 5.76 cm/s in NS (FN) component and 15.8 cm/s, 10.8 cm/s and 11.01 cm/s in EW (FP) component, respectively. As compared, NS (FN) values are larger than the EW (FP) except for the station Bitlis-dsi. Bitlis-dsi has remarkably two times larger peak value in EW (FP) component than NS (FN). Effect of rupture is evident despite the r_{jb} distance of 82.8 km from the center of energy release. If the PSA and PSV with 5% critical damping in Figs. 5 and 6 are re-evaluated one more time to distinguish the characteristics of the directivity effects. It is obvious that the NS (FN) component of Muradiye with PSV peaks oscillating between 25 and 50 cm/s with many large peaks reflects the propagation of the progressive rupture directivity. In contrast to FN, EW (FP) component also has same trend probably due to suitable dip and rake angles of the causative fault. PSA peak value of 600 cm/s^2 at the period of 0.4 s. is dominant for Muradiye in NS (FN) component and decreasing down at about 2 s. In the fault-parallel (EW) direction, station Muradiye has same peak characteristic with

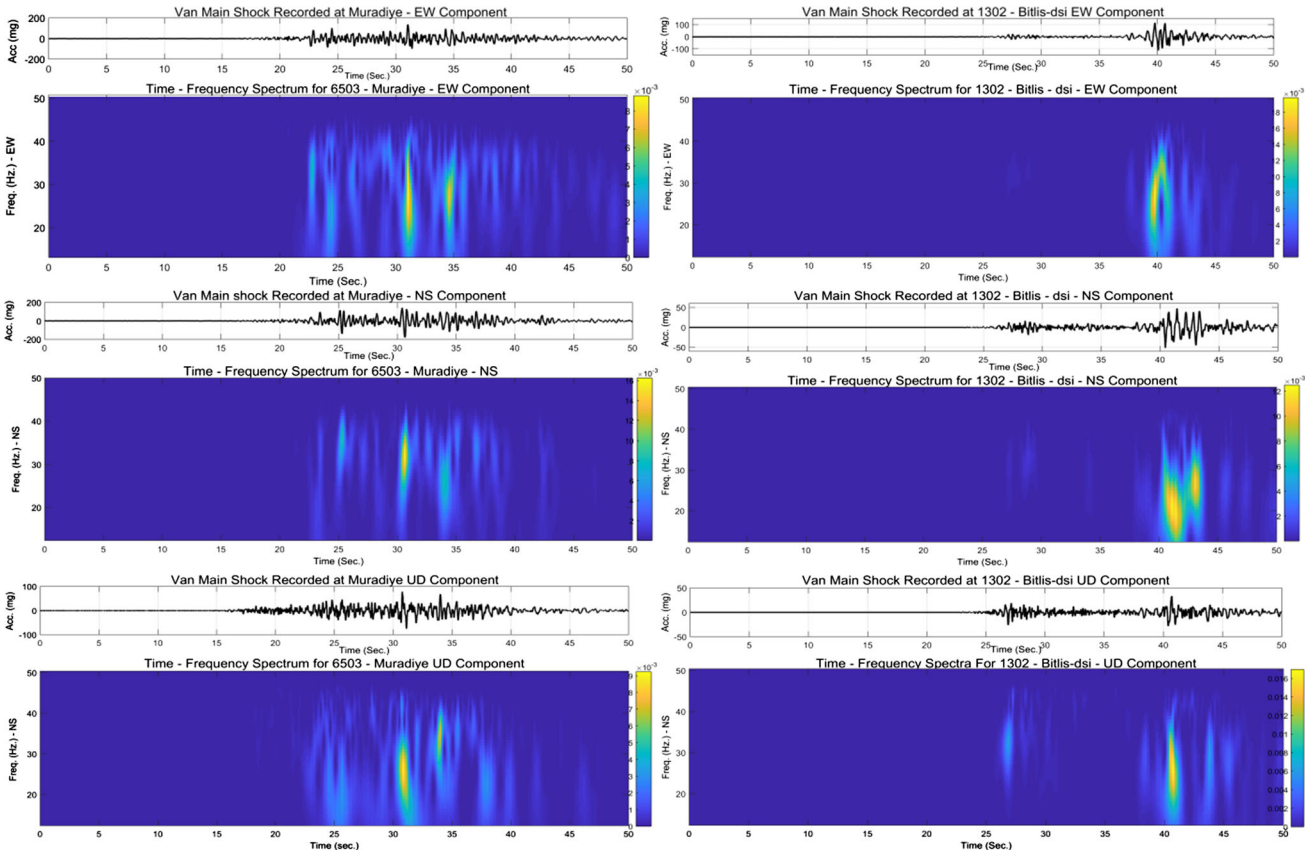
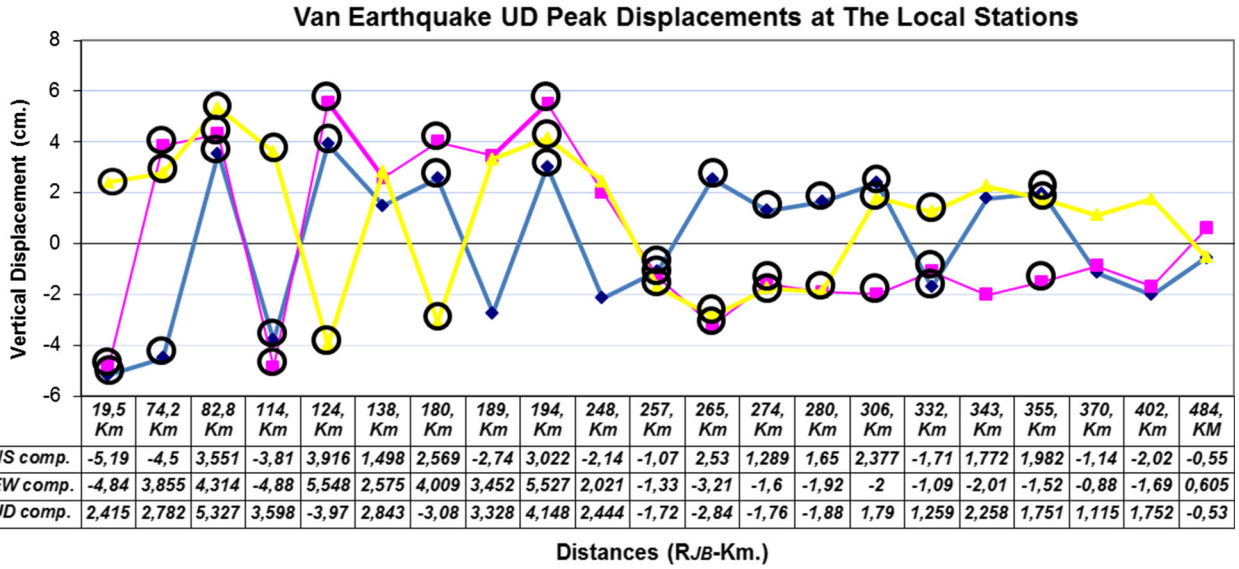


Fig. 12 Frequency–Time relations of the main shock recorded at Muradiye (left column) and Bitlis-dsi (right column). Velocity time histories high-pass-filtered at 2Hz

smaller values increasing up to 400 cm/s^2. Bitlis-dsi yields single PSV peak at 0.6 s, which is almost close to Muradiye. It is strong indicator declaring rupturing effect for the city of Bitlis-dsi with single spectral broadband peak larger than Muradiye in both velocity and acceleration spectra for the fault-parallel (EW) direction. Controversially fault-normal (NS) component have larger period band peaks at certain peak periods such as 0.5 s, 1 s and 2 s. In the FN (NS) direction, Bitlis-dsi has almost small peak values in the PSA and PSV spectra. For the vertical component, Muradiye is dominant over the other stations with broadband characteristic in PSA and PSV spectra. In spectral displacements, Muradiye has almost dominant peaks in both FN (NS) and FP (EW) components with the periods up to 2 s at where the city of Bitlis-dsi starts to become dominant. For the vertical (UD) component, peaks of the closest stations are interchangeably varying in the displacement spectra.

Site effects that appear with the broadband dominant peaks in the three components at the recording stations between 0.5 and 2 s (as shown in Fig. 5) may be removed to see the multiphase fracture possibility. On the other hand, waves with very low frequencies (i.e., 0.01–0.05–0.1 Hz) propagating from earthquake source cannot attenuate easily. After very short time, when another event is triggered; such low-frequency wave of the sub-event becomes subjected to intertwine with the previous one. Overlapping makes difficult to visually distinguish the sub-events. In contrast to low-frequency waves, high-frequency waves are attenuated in short time. Such a feature lets the high-frequency waves visually distinguishable in Time–Frequency analysis after filtering out the low-frequency content from the overlapped region. Therefore, recordings were high-pass-filtered at 2 Hz to relatively see the sub-event susceptibility from high-frequency content. Figure 12 shows velocity time histories and Time–Frequency contents for each component for Muradiye and Bitlis-dsi. Resultant Time–Frequency (T–F) spectra in Fig. 12 do not reflect the multiphase characteristic for the main shock. The oblique system generates the consistent energy distribution at the all recording stations in two horizontal components, which yield so far close frequency content at the corresponding times. P- and S-wave groups are seen propagating at the same instant in all stations with energy increase up to 50 Hz at the onset times of P and S waves.



	19,5 Km	74,2 Km	82,8 Km	114, Km	124, Km	138, Km	180, Km	189, Km	194, Km	248, Km	257, Km	265, Km	274, Km	280, Km	306, Km	332, Km	343, Km	355, Km	370, Km	402, Km	484, KM
NS comp.	-5,19	-4,5	3,551	-3,81	3,916	1,498	2,569	-2,74	3,022	-2,14	-1,07	2,53	1,289	1,65	2,377	-1,71	1,772	1,982	-1,14	-2,02	-0,55
EW comp.	-4,84	3,855	4,314	-4,88	5,548	2,575	4,009	3,452	5,527	2,021	-1,33	-3,21	-1,6	-1,92	-2	-1,09	-2,01	-1,52	-0,88	-1,69	0,605
UD comp.	2,415	2,782	5,327	3,598	-3,97	2,843	-3,08	3,328	4,148	2,444	-1,72	-2,84	-1,76	-1,88	1,79	1,259	2,258	1,751	1,115	1,752	-0,53

Fig. 13 Peak displacements in UD component increase with increasing distances (r_{jb}) on the Hanging wall site recording stations up to 200 km. Peak displacement values are tabulated below the graphic. Hanging wall sites are indicated by black circles

3.5 Importance of the Vertical Component for Structural Behavior

Characteristics of the vertical component of Van earthquake show comparatively significant effects than those of the lateral slip earthquakes. In Figs. 5, 6, 7 and 13, the vertical component has broadband characteristic, and it should not be ignored for the structures to be designed ordinarily for life safety performance level with reduction factor of 8. When compared to the vertical peaks of the lateral slip earthquakes, vertical component becomes important as much as the horizontal component. In Fig. 7, articulating spectral displacement demands get higher and may reach the critical values for structures with large fundamental periods like viaducts on highways, towers or any engineering structures subjected to large stiffness degradation during the damage. Such an extreme demand leads to shear failure and the loss of axial load carrying capacity. Structures produce different responses according to unfavorable structural configurations such as soft and weak stories, discontinuous structural system, variation in perimeter strength and abrupt drop in story stiffness between the floors. In addition to such irregularities, low quality in construction labor and poor material quality make worse the present condition. Structural vulnerability arises when buildings have such unfavorable conditions. Figure 13 shows the distribution of the vertical peak displacement values with respect to distances (r_{jb}). It is noticeable that UD peak values increase between $+6$ and -6 cm with increasing distances (r_{jb}) up to 200 km on the Hanging wall site and extending considerably between $+3$ and -3 cm beyond 200 km. Hanging wall site stations are indicated by black circles.

V/H spectral ratios are computed for 5% damping for the main shock recorded by 22 stations to examine the effect of the vertical component. Bold black solid and dashed lines show the median spectral ratio and $\pm$ standard deviations, respectively, in Fig. 14. The logarithmic standard deviations do not change significantly by the frequencies from one component to another. The median spectral ratio at 0.2 Hz is about 0.75 and it is 0.7 at 1 Hz. The scatter is almost same for both directions. The V/H spectral ratios of Muradiye at 0.2 Hz ($T = 5$ s) and 5 Hz ($T = 0.2$ s.) are 0.5 and 1, respectively for EW (FP) direction. For the NS (FN) direction, Muradiye yields 0.8 at 0.2 Hz ($T = 5$ s) and 0.65 at 5 Hz ($T = 0.2$ s). Spectral ratios show that the vertical peak spectral acceleration is larger than the horizontal peak spectral acceleration in the low-frequency region (0.2–1 Hz) for the distant sites like stations 6901, 2902, 2307, 4404 and 2305 as seen in Fig. 14 and it is changing between 1 and 1.5 for NS (FN) direction, and between 1 and 2.5 for EW (FP) direction. It might be concluded that the V/H ratio is strongly dependent on frequency content, site-to-source distance and site condition. The V/H ratio notably tends to exceed the rule-of-thumb value of 2/3 at the small frequencies (long periods) and approaches to 2/3 in the intermediate period range for the distant stations. Bitlis-dsi with 82.8 km of r_{jb} behaved differently. In EW (FP) direction, V/H spectral ratios for the frequencies after 1 Hz are lower than median mines standard deviations (about 0.175) and it is seen that the city in the direction of rupturing received very strong horizontal spectral accelerations in EW (FP) direction.

The vertical spectral accelerations are on average 0.7 times their corresponding horizontal peak spectral values. Such ratio is when compared with the code proposed uni-

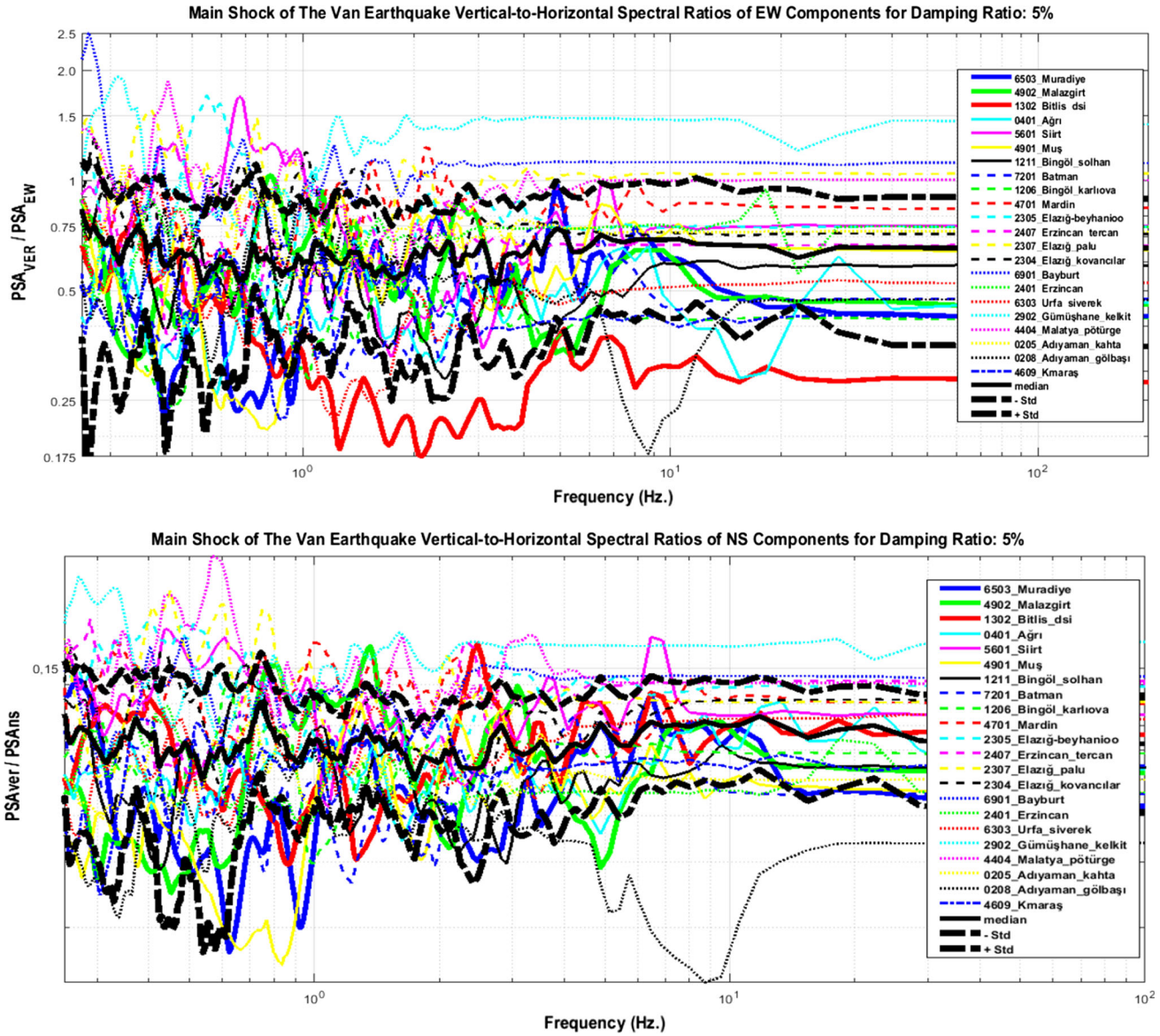


Fig. 14 Vertical-to-horizontal spectral ratios for 5% spectral damping ratio, top for EW (FP) direction, low for NS (FN) direction

directional design spectrum, presence of such a vertical earthquake within the range of the structural periods may significantly increase the moment demand even if the lateral forces decrease. Furthermore, horizontal spectral values are reduced by dividing with a strength reduction factor R, 4 or 8 for nominal or high level of ductility. Such a constant strength reduction factor for both horizontal and vertical directions implying same level of ductility will not be realistic. Design codes are intended to provide a conservative bound for the shear strength and are not suited to address the member capacity under varying axial load. Based on a large body of available studies [41], vertical oscillation may lead to axial force variation in column member and a noteworthy reduction in shear capacity. Degradation of shear strength due to inelastic cycles can lead to progressive member failures and finally it reduces the ductility capacity of structural system.

4 Discussion on Seismic Conceptual Design of RC Building

Regulations provide that structural strength during earthquake could be maintained without excessive degradation. In fact, seismic design codes are inadequate to quantify that the structural strength provided by the codes is not exceeded by the earthquake demand. In the earthquake-resistant design, it is preferable to consider forces generated

by earthquake-induced displacements rather than traditional loads. For reinforced concrete (RC) structures, to prevent inelastic shear deformations, required shear strength must be greater than required flexural strength. In ductile design, the structure is expected to deform to eight times the calculated deformation for instance for $R = 8$. Under large deformations, columns could be expected to develop over strength moments. Recently in capacity design philosophy, inelastic bending deformations may lead to failure and ductility can be considered the vital attribute of maintaining strength during reversible inelastic deformations. Depending on the configuration of the structural frame system, undesirable inelastic deformation might be intensified in comparison with the code predicted inelastic deformations.

As observed in the field, due to opening the ground floor to the maximum extent for possible shopping or parking requirements, soft story failures were the most common causes of failure in the town of Ercis and Van. Column sway mechanism at the basement developed high local ductility demand. Under ductile response to the earthquake, high compression strains are expected from the combined effects of axial force and bending moment. As observed adequate, closely spaced and well-implemented transverse reinforcements (i.e., stirrups) were not placed regularly in the potential plastic hinge region in column confinement zones at the base and top ends. Buckling of the longitudinal reinforcement, shear failures both within and outside the plastic hinge zone and weak beam-strong column design philosophy to dissipate seismic energy as enforced by the building code should be implemented strictly in engineering day practice to stop undesirable failure modes.

A–D spectra reflect the amplification potential of the ground motion produced by the building response due to uncontrolled high ductile frame behavior. Building response with low rigidity because of bad construction practice produces displacement exceeding capacity of the structure and starting progressive failure. On more precisely, differences in site responses between two hanging wall and footwall blocks may make buildings in Erciş more susceptible to failure than those in other towns in the Van region.

Many existing RC buildings in the town of Erciş as observed in other towns in the region may have been designed without complete consideration for the capacity design of RC frames and did not incorporate the special or good detailing that is essential for ductile concrete frame on the site. As known well from inelastic design, high ductile frame experiences a loss in stiffness and increases deflection of the structure, which may develop failure state even in low peak ground accelerations. Depending on the available ductility capacities that construction practice in the region formed, damage is intensified thoroughly. These spectral acceleration and displacement demand is easily estimated at the design stage from the point at which the capacity curve of the structure intersects the earthquake demand curve with a close damping ratio. As known well, at longer periods, the displacement spectrum is constant and consequently acceleration spectrum in the long-period region decreases with the square of the period T. Depending on the earthquake and site characteristics, the constant displacement band of the spectrum may begin at even at shorter periods like at about 2 s, which is shorter than expected periods. In the very long-period region, spectral displacements decrease to the value of the peak ground displacement [24]. Therefore, it is not always safe in design that the columns, which are designed to resist horizontal forces and displacement is limited to code allowable small displacement. The columns, which have to carry the gravity loads, should, however, be able to follow the horizontal displacements of the structure without losing their load bearing capacity under uncontrollable hysteretic responses. Global failure for the RC structures as observed at the site might be assumed based on designed interstory drift ratio capacity under nonlinear structural response when exceeded by the earthquake demand and the progressive side-sway collapse mechanism. In Turkish Earthquake Code (TEC, 2007) the immediate occupancy, life safety and collapse prevention drift limits are defined as 1%, 3% and 4% of maximum interstory drift ratios, respectively. Code proposed limits might vary actually from different seismic activities/mechanisms, variability in the data sets or interference between ground motions and structural behavior. Depending on soil condition (soft and stiff sites), effect of foundation stiffness on capacity of the building can also be pronounced for the roof displacement of flexible support since it is known that the top displacement of flexible support is relatively higher than of fixed support due to additional rotation and displacement allowed by the flexible support.

5 Conclusions

Everek erosional reverse fault produced the largest recorded seismic event in the collision tectonic regime of the Eurasia and Arabian plates. Seismotectonic characteristics have been identified by peculiar evidence, if compared with the conventional knowledge inferred from lateral slip mechanism earthquakes. Processing of a large number of strong motion recordings in the fault-normal (FN) and fault-parallel (FP) directions emphasizes hanging wall effect, source, rupturing, directivity and propagation effects. Reverse-oblique earthquake that is not considered clearly in current design regulations portraits the following results,

1. Hanging wall effects are observed as the increase in ground motion peaks at short distances for the stations on the hanging wall side of the ruptured fault and such increments are not seen at the same closest distance sta-

tions on the other side. The hanging wall effect is caused by a combination of radiation pattern, source directivity and the entrapment of seismic waves within the hanging wall wedge of the fault [2].

2. Although the recorded PGA values are small, effects of directivity and hanging wall effect increased the influence of the seismic loading. The V/H spectral ratio exceeds the traditionally accepted ratio of 2/3 at the long periods. Such a ratio causes axial force variation in column member and significant reduction in shear capacity. Degradation of shear strength can lead to progressive member failures in turn and finally it reduces the ductility capacity of structural system. Characteristics of the vertical ground motion, especially in the direction of the rupturing zone, have excessive effects to the engineering structures, therefore horizontal and vertical components of the earthquake might be considered equally. Furthermore, coupled effect is also a reality in practice as discussed in the text and should be considered in structural design as enforced by the new Turkish Earthquake Code.
3. Elastic design spectrum well envelopes the spectral values computed from recordings of the reverse fault causative earthquake. However, for inelastic design spectrum that is exceeded many times in the entire region, code enforcing inelastic design with either nominal or high level of ductility essentially requires complete construction quality implementing constructive details. Responses of the majority of the buildings in the town of Erciş with typical fundamental periods between 0.3 and 1.0 s exhibit the inelastic structural behavior under the forward directivity of the fault rupture in the east–west direction. In the region, construction quality is not appropriate to meet the requirements for ductile behavior of the structure. Hence important number of the structures received damage.
4. Bitlis-dsi in front of the direction of the rupturing received displacements from S-wave pulses, surface waves with larger periods. Ground displacements in the particle motion plots associated directly with the process of the fault rupture is distinct from other types of the long-period surface motions at the sites such as shear wave pulses and elliptical retrograde Rayleigh pulses.
5. From acceleration–displacement plot of the main shock, in Erciş, it is deduced that the structures were undergone excessive accelerations under the effect of the hanging wall and directivity and received severe structural damages, which cause the dominant periods become longer. In turn, large displacements accelerated the collapse mechanism.
6. Malazgirt which is close to the Far East end of the causative fault system seems to be under the backward effect. Erciş with a distance almost equal to Muradiye might be received similar PGA values comparable to Muradiye because of the similarities in source-to-site distance, soil class, propagation effect and fault zone characteristics.
7. Van should be received small values of acceleration during the main shock due to footwall characteristic, although the city has similar epicentral distance like Muradiye and located in the fault-normal direction.

Although the area is seismically active region and subject to the thrust fault triggering catastrophic earthquake potential, there is no sufficient instrumentation in the region to better understand the source and site characteristics for engineering usage. New wider large instrumentation program for the region among the regional countries seems to be necessary.

References

1. Koçyiğit, A.: New field and seismic data about the intraplate strike-slip deformation in Van region, East Anatolian Plateau, E Turkey. J. Asian Earth Sci. **62**, 586–605 (2013)
2. Beyen, K.; Tanırcan, G.: Strong motion characteristics of the 2011 Van earthquake of Turkey: implications of seismological aspects on engineering parameters. Earthq. Struct. **8**(6), 1363–1386 (2015)
3. Çoşkan, S.; Kartal, M.E.; Bilir, T.: The effect of concrete strengths obtained from 2011 Van earthquake on the structural performance of RC buildings. Arab. J. Sci. Eng. **41**, 3817–3825 (2016)
4. Ilki, A.; Celep, Z.: Earthquakes, existing buildings and seismic design codes in Turkey. Arab. J. Sci. Eng. **37**, 365–380 (2012)
5. Ozden, S.: Performance of precast concrete structures in October 2011 Van earthquake, Turkey. Mag. Concr. Res. **66**(11), 543–552 (2014)
6. Tapan, M.; Comert, M.; Demir, C.; Sayan, Y.; Orakcal, K.; Ilki, A.: Failures of structures during the October 23, 2011 Tabanlı (Van) and November 9, 2011 Edremit (Van) earthquakes in Turkey. Eng. Fail. Anal. **34**, 606–628 (2013)
7. Akansel, V.; Ameri, G.; Askan, A.; Caner, A.; Erdil, B.; Kale, Ö.; Okuyucu, D.: The 23 October 2011 Mw 7.0 Van (Eastern Turkey) earthquake: interpretations of recorded strong ground motions and post earthquake conditions of nearby structures. Eq. Spectra **30**, 657–682 (2013)
8. Taskin, B.; Sezen, A.; Tugsal, U.M.; Erken, A.: The aftermath of 2011 Van earthquakes: evaluation of strong motion, geotechnical and structural issues. Bull. Earthq. Eng. **11**(1), 285–312 (2013)
9. Taymaz, T.; Yilmaz, Y.; Dilek, Y.: The Geodynamics of the Aegean and Anatolia: Introduction, vol. 291, pp. 1–16. Special Publication-sGeological Society, London (2007)
10. Barka, A.A.; Reilinger, R.: Active tectonics of the Eastern Mediterranean Region: deduced from GPS, neotectonic and seismicity data. Ann. Geophys. **40**(3) (1997). https://doi.org/10.4401/ag-3892
11. Mc Clusky, S.; Balassanian, S.; Barka, A.; et al.: GPS constraints on plate kinematics and dynamics in the Eastern Mediterranean and Caucasus. J. Geophys. Res. Atmos. **105**(B3), 5695–5719 (2000)
12. Doğan, B.; Karakaş, A.: Geometry of co-seismic surface ruptures and tectonic meaning of the 23 October 2011 M_w 7.1 Van earthquake (East Anatolian Region, Turkey). J. Struct. Geol. **46**, 99–114 (2013)

13. Elliot, J.R.; Copley, A.C.; Holley, R.; Scharer, K.; Parsons, B.: The 2011 M_w 7.1 Van (Eastern Turkey) Earthquake. J. Geophys. Res. Solid Earth **118**, 1–19 (2013)
14. Kalafat, D.; Güneş, Y.; Kekovalı, K.: 2 Jully 2004 Doğubayazıt (Karaköse-Ağrı) earthquake, preliminary field report. Council of Europe, EMSC European Mediterranean Seismological Centre, Special web pages on significant earthquakes. www.emsc-csem.org (2004). Accessed 11 Sept 2018
15. Kalafat, D.; Kekovalı, K.; Güneş, Y.; Küsmezer, A.; Garip P.; Berberoğlu, A.; Bekler, F.: 25 January 2005 Hakkari Earthquake report. Council of Europe, EMSC European Mediterranean Seismological Centre, Special web pages on significant earthquakes. www.emsc-csem.org (2005). Accessed 11 Sept 2018
16. Taymaz, T.; Eyidoğan, H.; Jackson, J.: Source parameters of large earthquakes in the East Anatolian fault zone (Turkey). Geophys. J. Int. **106**, 537–550 (1991). Oxford
17. Gülkan, P.; Gürpınar, A.; Celebi, M.; Arpat, E.; Gencoglu, S.: Engineering Report on the Muradiye–Çaldıran, Turkey, Earthquake of 24 November 1976. National Academy of Sciences, Washington (1978)
18. Gökkaya, K.: Geographic analysis of earthquake damage in Turkey between 1900 and 2012. Geomat. Nat. Hazards Risk **7**(6), 1948–1961 (2016)
19. AFAD: Deprem Dairesi Başkanlığı. http://www.deprem.gov.tr (2011). Accessed 11 Sept 2018
20. KOERI:http://www.koeri.boun.edu.tr/Publications/OCTOBER%2023,%202011%20VAN%20EARTHQUAKE_14_262.depmuh (2011). Accessed 11 Sept 2018
21. NERA: Analysis of relative contribution of source, scattering and local site effects to ground motion, Network of European Research Infrastructures for Earthquake Risk Assessment and Mitigation, Project in JRA3—Work Package, EC Project number: 262330 (2013)
22. Konagai, K.; Ulusay, R.; Kumsar, H.; Aydan, Ö.; Çelebi, M.: The characteristics of seismic, strong motion and structural damage of the 2011Van-Erciş earthquake. In: Proceedings of the International Symposium on Engineering Lessons Learned from the 2011 Great East Japan Earthquake, pp. 1902–1913, Tokyo, 1–4 Mar 2012
23. MATLAB 8.2: The MathWorks Inc., Natick, MA (2008)
24. Spudich, P.; Joyner, W.B.; Lindh, A.G.; Boore, D.M.; Margaris, B.M.; Fletcher, J.: B: SEA99: a revised ground motion prediction relation for use in extensional tectonic regimes. BSSA **89**(5), 1156–1170 (1999)
25. Abrahamson, N.A.: Effects of rupture directivity on probabilistic seismic hazard analyses. In: Proceedings of the Sixth International Conference on Seismic Zonation, Earthquake Engineering Research Institute, Palm Springs, pp. 151–156 (2000)
26. Abrahamson, N.A.; Silva, W.J.: Summary of the Abrahamson & Silva NGA ground-motion relations. Earthq. Spectra **24**(1), 67–97 (2008)
27. Boore, D.M.; Atkinson, G.M.: Ground-motion prediction equations for the average horizontal component of PGA, PGV, and 5% damped PSA at spectral periods between 0.01s and 10.0s. Earthq. Spectra **24**(1), 99–138 (2008)
28. Campbell, K.W.; Bozorgnia, Y.: NGA ground motion model for the geometric mean horizontal component of PGA, PGV, PGD and 5% damped linear elastic response spectra for periods ranging from 0.01 to 10s. Earthq. Spectra **24**(1), 139–171 (2008)
29. Chiou, B.S.J.; Youngs, R.R.: NGA ground motion relations for the geometric mean horizontal component of peak and spectral ground motion parameters. Earthq. Spectra **24**(1), 173–215 (2008)
30. McVerry, G.H.; Zhao, J.X.; Abrahamson, N. A.; Somerville, P. G.: Crustal and subduction zone attenuation relations for New Zealand earthquakes. In: Proceedings of 12th World Conference on Earthquake Engineering, Paper No. 1834, Auckland (2000)
31. Field, E.H.; Jordan, T.H.; Cornell, C.A.: OpenSHA: a developing community-modeling environment for seismic hazard analysis. Seismol. Res. Lett. **74**(4), 406–419 (2003)
32. Shabestari, Khosrowi T.; Yamazaki, F.: Near-fault spatial variation in strong ground motion due to rupture directivity and hanging wall effects from the Chi–Chi, Taiwan earthquake. Earthq. Eng. Struct. Dyn. **32**, 2197–2219 (2003)
33. TEC: Ministry of public works and settlement, Specification for structures to be built in disaster areas, Republic of Turkey (2007)
34. Fajfar, P.: A nonlinear analysis method for performance based seismic design. Earthq. Spectra **16**(3), 573–592 (2000)
35. Ulusay, R.; Kumsar, H.; Konagai, K.; Aydan, Ö.: The characteristics of geotechnical damage by the 2011 Van-Erciş earthquake. In: Proceedings of the International Symposium on Engineering Lessons Learned from the 2011 Great East Japan Earthquake, Tokyo (2012)
36. Somerville, P.G.; Smith, N.F.; Graves, R.W.; Abrahamson, N.A.: Modification of empirical strong ground-motion attenuation relations to include the amplitude and duration effect of rupture directivity. Seismol. Res. Lett. **68**(1), 199–222 (1997)
37. Chopra, A.K.; Chintanapakde, C.: Comparing response of SDF systems to near-fault and far-fault earthquake motions in the context of spectral regions. Earthq. Eng. Soil Dyn. **30**, 1769–1789 (2001)
38. Akkar, S.; Yazgan, U.; Gulkan, P.: Drift estimates in frame buildings subjected to near-fault ground motions. J. Struct. Eng. **131**(7), 1014–1024 (2005)
39. Champion, C.; Liel, A.: The effect of near-fault directivity on building seismic collapse risk. Earthq. Eng. Struct. Dyn. **41**, 1391–1409 (2012)
40. Somerville, P.G.: Magnitude scaling of the near fault rupture directivity pulse. Phys. Earth Planet. Inter. **137**, 201–212 (2003)
41. Kunnath, S.K.; Abrahamson, N.; Chai, Y.H.; Erduran, E.; Yilmaz, Z.: Development of guidelines for incorporation of vertical ground motion effects in seismic design of highway bridges. Technical report CA/UCD-SESM-08-01 (2008)